The Company of **Biologists**

RESEARCH ARTICLE

Mitochondrial import, health and mtDNA copy number variability seen when using type II and type V CRISPR effectors

Zuriñe Antón[1], Grace Mullally[2], Holly C. Ford[2], Marc W. van der Kamp[3,4,5], Mark D. Szczelkun[2,5,*] and Jon D. Lane[1,5,*]

ABSTRACT

Current methodologies for targeting the mitochondrial genome for research and/or therapy development in mitochondrial diseases are restricted by practical limitations and technical inflexibility. A molecular toolbox for CRISPR-mediated mitochondrial genome editing is desirable, as this could enable targeting of mtDNA haplotypes using the precision and tuneability of CRISPR enzymes. Such 'MitoCRISPR' systems described to date lack reproducibility and independent corroboration. We have explored the requirements for MitoCRISPR in human cells by CRISPR nuclease engineering, including the use of alternative mitochondrial protein targeting sequences and smaller paralogues, and the application of guide (g)RNA modifications for mitochondrial import. We demonstrate varied mitochondrial targeting efficiencies and effects on mitochondrial dynamics/function of different CRISPR nucleases, with *Lachnospiraceae* bacterium ND2006 (Lb) Cas12a being better targeted and tolerated than Cas9 variants. We also provide evidence of Cas9 gRNA association with mitochondria in HeLa cells and isolated yeast mitochondria, even in the absence of a targeting RNA aptamer. Our data link mitochondrial-targeted LbCas12a/crRNA with increased mtDNA copy number dependent upon DNA binding and cleavage activity. We discuss reproducibility issues and the future steps necessary for MitoCRISPR.

KEY WORDS: MitoCRISPR, Cas9, Cas12a, gRNA, crRNA, Targeting, Import

INTRODUCTION

Mitochondria are crucial for the maintenance of cellular energy levels. In humans, all 37 genes contained within mitochondrial DNA (mtDNA) encode or aid biosynthesis of proteins involved in the OXPHOS pathway (DiMauro and Schon, 2003). Despite mtDNA contributing only ∼1% of mitochondrial proteins – the remainder being encoded in the nucleus – four of the five OXPHOS complexes contain mtDNA-encoded subunits. Consequently, mutations in both nuclear and mitochondrial genomes can result in mitochondrial diseases with a range of clinical manifestations.

Mitochondrial diseases are currently incurable, with a lack of understanding of the complexities of mitochondrial genetics and mitochondrial biology impeding identification of targets for the development of treatments (Rahman and Rahman, 2018). Existing therapies mainly focus on symptom management through exercise and dietary supplements (Chicani et al., 2013; DiMauro and Hirano, 2009). Thus, the development of mitochondrial molecular genetics techniques that could be used therapeutically for mitochondrial diseases remains an important challenge.

Inherited disease-causing mtDNA mutations have been shown to be either homoplasmic, where near to 100% of mtDNA copies carry the mutation, or heteroplasmic, where the mutation is carried by a subset of the total mtDNA. In general, mutation load above ∼70% is required to present a severe phenotype, although this threshold is disease specific. Molecular tools to edit mtDNA in order to correct disease-associated mutations are particularly desirable, and this approach has now been demonstrated using a split bacterial deaminase (DddA) for targeted C/G to T/A conversions in double-stranded (ds)DNA (Mok et al., 2020). While this method is in its infancy, the field has developed targeted endonucleases to produce dsDNA breaks in mtDNA haplotypes, which are then degraded by the mitochondria rather than being repaired (Moretton et al., 2017; Peeva et al., 2018). The remaining wild-type (WT) mtDNA then replicates to re-establish mtDNA copy number. This 'heteroplasmy purification' has been successfully demonstrated in cell culture and in mouse models using restriction endonucleases (MitoREs), zinc finger nucleases (MitoZFNs), TALENs (MitoTALENs) and homing endonucleases (Gammage et al., 2018; Patananan et al., 2016). However, although independently validated (Phillips et al., 2017), these tools are impracticable and not widely adopted, because (i) REs match few clinical mutations and cannot be readily re-engineered (Bogdanove et al., 2018), and they additionally have high 'off-target' cleavage rates (Bayona-Bafaluy et al., 2005; Srivastava and Moraes, 2001); (ii) ZFNs require rounds of protein engineering/refinement; (iii) assembly of TALE parts is hindered by problematic cloning of DNA repeats; and (iv) TALENs and ZFNs can have low import efficiency, and can be mis-trafficked (e.g. ZFs have internal nuclear targeting sequences) (Hashimoto et al., 2015; Minczuk et al., 2006; Moraes et al., 2014). To overcome some of these difficulties, we have investigated the use of a re-engineered flexible version of the CRISPR method for mitochondrial genome manipulation (Fig. 1A).

CRISPR systems have revolutionised molecular genetics by providing a quick and convenient method to efficiently target proteins to almost any short DNA sequence (Sternberg and Doudna, 2015). In this system, CRISPR guide (g)RNAs target effector nucleases to form a DNA/RNA hybrid (R-loop) at the target sequence, displacing the non-complementary DNA strand and cleaving the two strands of DNA. Binding is assisted by a protospacer adjacent motif (PAM) that is recognised by the

[1]Cell Biology Laboratories, School of Biochemistry, Faculty of Life Sciences, University of Bristol, Bristol BS8 1TD, UK. [2]DNA-Protein Interactions Unit, School of Biochemistry, Faculty of Life Sciences, University of Bristol, Bristol BS8 1TD, UK. [3]School of Biochemistry, Faculty of Life Sciences, University of Bristol, Bristol BS8 1TD, UK. [4]Centre for Computational Chemistry, School of Chemistry, Faculty of Science, University of Bristol, Bristol BS8 1TD, UK. [5]BrisSynBio, Life Sciences Building, Tyndall Avenue, University of Bristol, Bristol BS8 1TQ, UK.

*Authors for correspondence (jon.lane@bristol.ac.uk; mark.szczelkun@bristol.ac.uk)

Z.A., 0000-0002-0175-8548; M.W.v.d.K. , 0000-0002-8060-3359; M.D.S., 0000-0002-2501-6602; J.D.L., 0000-0002-6828-5888
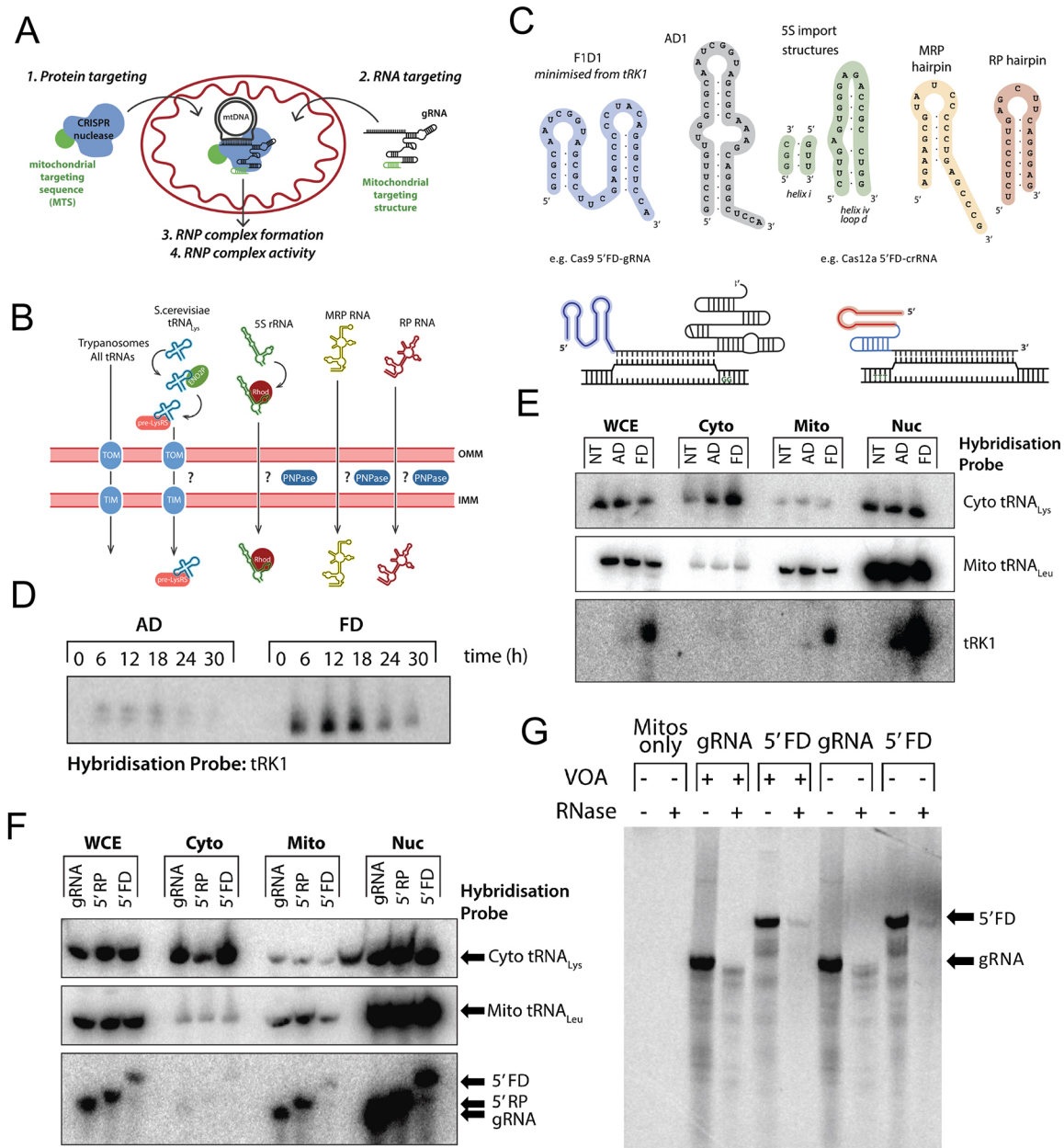
Fig. 1. Import of Cas9 gRNAs into mitochondria in HeLa cells or isolated yeast mitochondria. (A) The main steps required for the development of a working MitoCRISPR system. (B) Natural RNA import mechanisms in Trypanosomes, *S. cerevisiae* and mammals. (C) Minimised RNA import motifs that have been identified for tRK1, 5S rRNA, MRP RNA and RP RNA, and are capable of directing RNA sequences of interest into mitochondria. Two examples are shown for Cas9 gRNAs and Cas12a crRNAs modified with 5′FD and 5′RP, respectively. (D) Transfection time course for AD and FD RNA. (E) Northern blotting of HeLa cells for AD and FD separated by urea-PAGE, transferred onto nitrocellulose membrane and probed against tRK1 probe. (F) Northern blotting for cells transfected with either unmodified gRNA, or gRNA modified with 5′RP or 5′FD. The three blots represent different northern probes: cytoplasmic tRNA$_{Lys}$ (top); mitochondrial tRNA$_{Lys}$ (middle); or gRNA (bottom). The different mobilities of the gRNA are due to the differences in size when RP or FD aptamers are present. (G) Import of radiolabelled RNA into isolated yeast mitochondria. TRIzol-extracted RNA was separated on urea-PAGE gels. Following separation, gels were fixed, dried and exposed to a phosphor screen. WCE, whole-cell extract; Cyto, cytoplasmic; Mito, mitochondrial; Nuc, nuclear.

CRISPR nuclease. There are several CRISPR-Cas system types from different species, of which the type II *Streptococcus pyogenes* (Spy) Cas9 and *Staphylococcus aureus* (SaCas9), and type V *Lachnospiraceae bacterium* (Lb) Cas12a and *Acidaminococcus sp.* (As) Cas12a have been tested in this study. Cas9 has been widely used for genome engineering. It comprises two nuclease domains, the RuvC-like and HNH domains, which generate blunt-ended DNA double strand breaks (DSBs) (Jinek et al., 2012; Mojica et al., 2009). Cas12a, also referred to as Cpf1, contains a single RuvC

endonuclease domain that cleaves the two DNA strands in turn, resulting in a staggered DSB with a 5′ overhang (Swarts, 2019).

Steps towards development of CRISPR machinery for mtDNA have been described by others. Jo et al. first introduced a standard nuclear targeted CRISPR/Cas9 system to edit mtDNA (Jo et al., 2015). They unexpectedly reported that introducing nuclear-targeted Cas9 and unmodified gRNAs in HeLa cells resulted in mtDNA cleavage (Jo et al., 2015). However, there have not been any published applications of this tool, and attempts to reproduce

these data by us and by others (Pereira and Moraes, 2017) have not been successful. The second report was published by Orishchenko et al. using a FLAG–Cas9 targeted to fragmented mitochondria of viral-producing cells by appending a COX8A mitochondrial-targeting sequence (MTS) (Orishchenko et al., 2016; Verechshagina et al., 2019). The paper showed only one cell in which anti-FLAG colocalised with very fragmented mitochondria, and did not describe any experiments to address mitochondrial gRNA localisation. As with the Jo et al. work, these data have not yet been independently corroborated. A recent publication on MitoCRISPR attempted to add mitochondrial-targeting structures to the gRNA for the first time (Loutre et al., 2018). The authors showed a decrease in mtDNA copy number with COX8A-Cas9 and gRNAs modified to contain the targeting sequences from 5S RNAs. Two gRNAs were required to produce a reduction of mtDNA copy number; a single target gRNAs had no significant influence on mtDNA content. The work was carried out in a heteroplasmic cell line, but the authors did not observe a shift in heteroplasmy.

The explosion in gene editing research more widely has been driven by the simplicity, reproducibility and adaptability of CRISPR-Cas systems. Almost immediately after the first descriptions of CRISPR-Cas9, multiple labs demonstrated reliable gene editing by the facile recoding of a gRNA/crRNA spacer sequence. This has not so far been the case with MitoCRISPR. We suggest that 'leaky' mitochondria, possibly occurring during isolation, and/or failing mitochondrial proteostasis in Cas9-expressing cells, might explain some or all of the observations in these previous publications. It is critical that MitoCRISPR is fully characterised (mtDNA copy number reduction alone is not sufficient) and that there is clear evidence of reproducibility, validated by independent labs.

By designing and re-engineering several versions of CRISPR nucleases and gRNAs, including testing alternative MTSs, smaller paralogues, and the addition of mitochondrial targeting RNA aptamers, we have here assessed (i) CRISPR/Cas mitochondrial targeting and influence on mitochondrial dynamics/function; and (ii) DNA cleavage activity in a model mitochondrial disease cell line (mitochondrial encephalomyopathy, lactic acidosis and stroke-like episodes cytoplasmic hybrids; MELAS cybrids). We explored the requirements for Cas9 gRNA association with mitochondria, including the influence of targeting RNA aptamers. Our study shows that SpyCas9 can be localised to mitochondria, but with low efficiency and causing severe mitochondrial network damage. However, LbCas12a was found to be efficiently expressed and targeted to the mitochondrial matrix via the TOM/TIM pathway in WT or MELAS (cybrids). Finally, we present our attempts to demonstrate an effect on mtDNA of a mitochondrial-targeted LbCas12a/crRNA combination; while we observed increases in mtDNA copy number in the MELAS disease model cybrid, dependent upon DNA binding and cleavage activity, this had poor reproducibility across independent validations and stable or prolonged Cas12a expression had deleterious effects on respiration. Our data emphasise the importance of CRISPR enzyme and mitochondrial targeting strategy selection, and further highlight how manipulation of the mitochondrial genome can have unpredictable outcomes in living cells.

RESULTS
Design of a MitoCRISPR system – targeting the CRISPR-Cas9 system to mitochondria
The development of a reliable MitoCRISPR system requires: (i) the targeted delivery of a CRISPR nuclease to the mitochondria by fusion to a peptide MTS; (ii) mitochondrial targeting of a CRISPR gRNA, possibly through fusion to a mitochondrial targeting domain; (iii) formation of a functional CRISPR ribonucleoprotein (RNP) complex inside the mitochondrial matrix; and (iv) functional nuclease activity of the CRISPR RNP complex (Fig. 1A). For direct import of non-native proteins, a naturally occurring MTS is commonly cloned upstream of the protein of interest (Verechshagina et al., 2018). In the context of this project, CRISPR proteins were delivered as DNA, either stably expressed through incorporation into the genome, or transiently expressed from a transfected plasmid.

In contrast to the mitochondrial protein import pathway, the import of mitochondrial RNA is poorly understood (Gammage et al., 2018). Mitochondrial import of CRISPR gRNA/crRNA therefore emerges as the critical challenge of developing MitoCRISPR. Several studies have described methods to import RNA into mitochondria, either harnessing natural mitochondrial RNA import machineries, or through non-natural means (Fig. 1B,C) (Dovydenko et al., 2015; Kolesnikova et al., 2010; Niazi et al., 2013; Wang et al., 2015). It has been proposed that short structured RNA sequences [aptamers; e.g. from tRNAs, non-coding RNAs (ncRNAs) such as 5S ribosomal RNA, or the RNA component of RNase P] can be appended to an exogenous RNA for import (e.g. Comte et al., 2013; Loutre et al., 2018); however, there is no consensus of understanding, and the existence of a dedicated pathway for mitochondrial import of RNAs is debated (Dovydenko et al., 2015; Loutre et al., 2018). Several functional ncRNAs are believed to be imported into the mitochondria, including tRNAs, the 5S RNA, MRP RNA, RNaseP RNA and mitochondrial microRNAs (mitomiRs), and although whole transcriptome analyses of mitochondria and mitoplasts have confirmed the presence of these (Mercer et al., 2011; Sripada et al., 2012), their mechanisms of import are not fully explored. Mitochondrial RNA import pathways differ from one system to another. Trypanosomes import all their tRNAs through the TOM/TIM system, whereas *S. cerevisiae* import just one, tRNALys (Fig. 1B). Import of tRNALys involves the protein factors enolase (ENO2P) and pre-LysRS, the pre-cursor of the mitochondrial lysyl-tRNA, acting in concert with a functional protein import machinery (Entelis et al., 2006; Kamenski et al., 2010).

In mammalian cells, mitochondrial import of 5S ribosomal RNA (rRNA), mitochondrial RNase P RNA (MRP) and RNase P RNA (RP) occurs by unknown mechanisms, although evidence implicates factors including rhodanese (Rhod) in the case of the 5S rRNA (Magalhães et al., 1998; Smirnov et al., 2010, 2008), and possibly PNPase during 5S, MRP and RP RNA import (Fig. 1B) (Holzmann et al., 2008; Puranam and Attardi, 2001; Wang et al., 2012). Despite conflicting evidence on the existence and mechanisms of mammalian RNA import, several groups have proposed minimal structural motifs that are sufficient to direct import (Fig. 1C). The F1D1 RNA, derived from tRK1, is the structure found to have the highest import efficiency; a related control sequence, the AD RNA, does not have the same effect (Kolesnikova et al., 2010). Moreover, truncating RNase RP and MRP RNAs has allowed identification of similar ~20 nt RNA hairpins in both RP and MRP RNA that direct mitochondrial import. Attaching these hairpins into non-imported RNAs can target RNAs for import, as shown with GAPDH (Wang et al., 2010). For import of Cas9 gRNA or Cas12a crRNAs into mitochondria, we used either the FD, AD or RP motifs through attachment at the 5′ ends (Fig. 1B,C).

SpyCas9 gRNAs co-fractionate with mitochondria in HeLa cells and isolated yeast mitochondria both with and without a targeting aptamer

The subcellular localisation of modified Cas9 gRNAs was determined by northern blotting. A cytoplasmic RNA (tRNALys) and a mitochondrial RNA (tRNALeu) were used as control markers. Probes designed against the corresponding transfected gRNA are described in the Materials and Methods section. Cells were transfected with unmodified gRNA, gRNA with 5′RP, and gRNA with 5′FD, and the hybridisation signal was determined using a probe for the hairpin region of the gRNA (Fig. 1D,E). Strong signals for all three gRNAs were observed in the nuclear fraction and, to a lesser extent, the mitochondrial fraction (Fig. 1F). The 5′FD gRNA produced the weakest signal in the mitochondrial fraction, contrasting with a stronger signal for the unmodified gRNA. Note that the cytoplasmic tRNA probe also gave a signal for the mitochondrial fraction, and both cytoplasmic and mitochondrial tRNA probes gave strong nuclear fraction signals (Fig. 1F), possibly due to contaminating mitochondria retained during fractionation.

To provide a sensitive method for following RNA import into isolated mitochondria, gRNAs were *in vitro* transcribed with ^{33}P-UTP. Unmodified gRNA and a modified gRNA were incubated with mitochondria with or without a membrane potential (±VOA). This control was included in case the protein import pathway was somehow required for polynucleotide import. Following a 10-min incubation at 25°C, pelleted mitochondria were treated with RNase to degrade non-imported RNA. RNA was then extracted from the yeast import mix by TRIzol extraction, and samples were separated on urea-PAGE (Fig. 1G). Both unmodified and 5′FD modified gRNAs were protected from RNase-mediated digestion, presumably by the mitochondrial membrane(s) (Fig. 1G). We cannot determine whether the gRNA protection is due to RNA protection by membrane association or genuine import. The absence of altered levels of protection in the presence of VOA suggest that in either case the membrane potential does not play a role, also excluding a role for TOM/TIM import pathway.

Our results indicate that gRNA can appear to be associated with mitochondria regardless of whether an RNA import aptamer was attached or not. This could provide support for the possibility that MitoCRISPR can be achieved without targeted import of the RNA. However, we note that these assays do not report on RNA import to the matrix. What our results clearly show is that association with mitochondrial membranes can protect RNA from RNases.

SpyCas9 is localised to mitochondria with low efficiency and causes mitochondrial damage

SpyCas9 was expressed from human codon optimised genes in two formats (Fig. 2A) – as nuclear-targeted SpyCas9 (NLS–SpyCas9–GFP) and mitochondria-targeted SpyCas9 (MTS–SpyCas9–GFP). A control protein, mitochondria-targeted GFP (MTS–GFP), was also included (Fig. 2A). We first tested the N-terminal MTS from human cytochrome *c* oxidase subunit viii (COX8A), one of the most widely used signal peptides comprising a 29-residue helix. Different transfection conditions, cell fixation methods and mitochondrial markers were used to assess the targeting efficiency and influence of mitochondria targeted Cas9 in human hTERT RPE1 cells (Fig. 2B–I). Cells transiently transfected with MTS–GFP showed mitochondrial GFP localisation confirming the ability of the COX8A MTS to direct proteins to the mitochondria under our experimental conditions (Fig. 2B,C). Using MTS–SpyCas9–GFP, some GFP signal was observed in the mitochondria of RPE1 cells following a 19-h transfection (Fig. 2B); however, the signal was weak, and many cells still showed nuclear and cytosolic GFP fluorescence. As expected, NLS–SpyCas9–GFP was mostly localised to the nucleus (Fig. 2B,C). Over longer expression periods using MTS–Cas9–GFP (up to 48 h), mitochondrial morphology was disrupted, and the GFP signal became progressively cytosolic (Fig. 2C,D).

Detailed analysis confirmed expected levels of mitochondrial colocalisation for each of these constructs (Fig. 2E), and revealed that MTS–SpyCas9–GFP, but not NLS-SpyCas9-GFP, significantly impacted on mitochondrial properties, as assessed by cytoplasmic occupancy (density; Fig. 2F), and mitochondrial network integrity (branch length; Fig. 2D,G). Live imaging of hTERT RPE1 cells stained with MitoTracker Red, suggested that, in a proportion of cells transfected with MTS–SpyCas9–GFP, mitochondrial membrane potential was severely disrupted (Fig. 2H); however, upon quantifiction of MitoTracker fluorescence, no significant differences from MTS–Cas9–GFP controls were recorded within the population of MTS–SpyCas9–GFP-positive cells (Fig. 2I). Cell-to-cell variability in MitoTracker intensity was probably caused by differences in MTS–SpyCas9–GFP expression levels, although this was not directly assessed. In general, mitochondria in the NLS–Cas9–GFP expressing cells were healthier, despite showing higher expression levels (Fig. 2H; asterisk indicates lower exposure time). Taken together, these results indicate that SpyCas9 is not efficiently targeted to mitochondria, and where targeted, is disruptive to mitochondrial homeostasis.

Comparative analysis of the mitochondrial import of various CRISPR-Cas systems

The established approach to determine the best CRISPR effector for gene editing applications is by empirical testing. Consequently, to improve CRISPR nuclease targeting efficiency and avoid the mitochondrial damage seen with SpyCas9, we tested three effectors previously validated for other methods; hence, SaCas9, and the type V effectors, LbCas12a and AsCas12a, were re-engineered as human codon optimised genes, and appended to alternative MTSs. The comparative probability of constitutive mitochondrial import was predicted for each variant using online tools (Fig. S1). There was no expectation for these proteins to be naturally imported to mitochondria, but there might be potential intrinsic features that would affect this process. Fig. S1A shows the domain organisation of SpyCas9, SaCas9 and LbCas12a. The overall structure and organisation of Cas9 and Cas12a are quite different (Yamano et al., 2016). LbCas12a has a RuvC-like endonuclease domain that is similar to the RuvC domain of Cas9; however, LbCas12a does not have an HNH endonuclease domain. One of the main structural differences is that the N-terminus of LbCas12a adopts a mixed α/β structure that is distinct to the N-terminal α-helical recognition lobe of Cas9 (Fig. S1A). Thus, this part of the protein might influence import to mitochondria. Moreover, using a bioinformatic prediction tool for identifying putative mitochondrial pre-sequences and cleavage sites (Fukasawa et al., 2015), LbCas12a was suggested to have a much higher predisposition to be imported to mitochondria than the other CRISPR variants (Fig. S1B).

Other parameters that might affect the efficiency of mitochondrial import of a construct were also analysed (Fig. S1C–E). When analysing their size, relative charge and hydrophobicity, LbCas12a and SaCas9 were predicted to be imported more efficiently, as they are smaller, more positively charged and less hydrophobic than AsCas12a or SpyCas9 (Fig. S1C). This could explain the poor mitochondrial targeting efficiency shown with SpyCas9 (Fig. 2). Another parameter could be the linear charge distribution of the N-termini (Fig. S1D), since this will be the first region to be
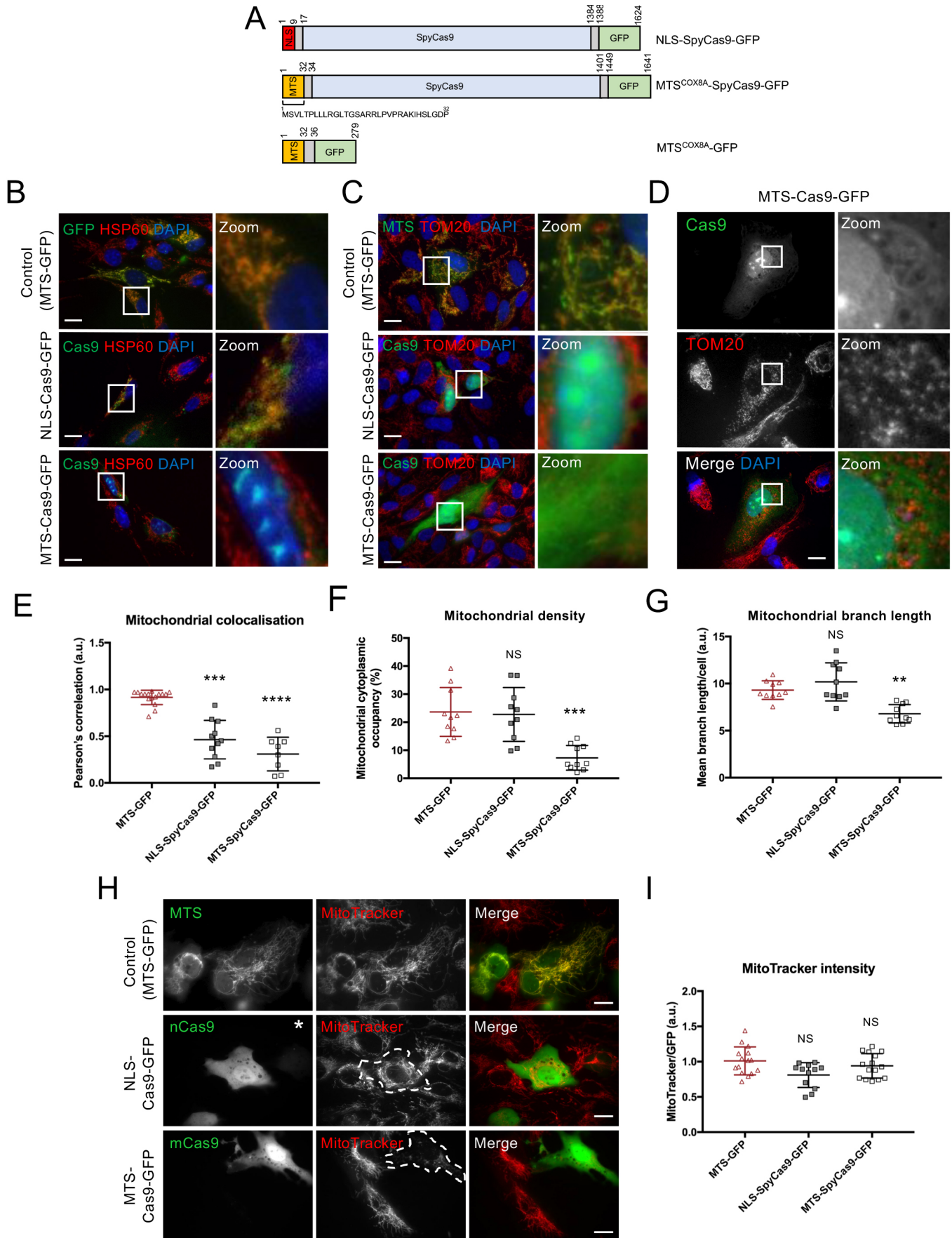
Fig. 2. See next page for legend.

Fig. 2. Low SpyCas9 mitochondrial import efficiency is observed using a standard targeting sequence in hTERT-immortalised human RPE1 cells. (A) Diagram representing the constructs used. The nuclear-targeting signal (MLS) is shown in red, the mitochondrial-targeting signal (MTS) in yellow, linkers in grey and GFP in green. (B) RPE1 cells transfected with MTS–Cas9–GFP, NLS–Cas9–GFP or MTS–GFP. Cells were fixed with −20°C methanol and stained with anti-HSP60 antibodies (19 h post transfection). Some cells also have nuclear or cytosolic GFP signal. (C) RPE1 cells transfected with MTS–Cas9–GFP, NLS–Cas9–GFP or MTS–GFP. Cells were fixed with formaldehyde and stained with anti-TOM20 antibodies (48 h post transfection). Cytosolic Cas9 localisation is observed after transfection with mitoCas9–GFP. (D) Fragmented mitochondria are observed in MTS–Cas9–GFP-expressing cells (48 h post transfection). (E–G) Analysis of mitochondrial parameters in RPE1 cells expressing MTS–GFP, NLS–Cas9–GFP or MTS–Cas9–GFP. (H–I) Analysis of mitochondrial membrane potential assessed by MitoTracker fluorescence). Example fields to the left, showing a cell (outlined in MitoTracker image) expressing MTS–Cas9–GFP with reduced membrane potential; quantification is shown to the right. (*)=10-fold lower exposure time was applied. Results are mean±s.d.; **$P<0.01$; ***$P<0.001$; ****$P<0.0001$; NS, not significant (one-way ANOVA with Tukey's test). Scale bars: 10 μm. a.u., arbitrary units.

imported. LbCas12a has a more positively charged N-terminus than SaCas9, so it could be more efficiently imported, whereas the latter is significantly smaller and has an overall more positive charge. We suggest that future studies might consider applying similar analysis to the expanding range of CRISPR effectors to help narrow the search for potential MitoCRISPR effectors. In terms of the MTS, we compared the COX8A MTS with the 69-residue MTS from *Neurospora crassa* ATPase subunit 9 (Su9) (Hartl et al., 1989; Westermann and Neupert, 2000), and a cryptic, internal 42-residue MTS from mammalian ATG4D, located immediately downstream of a caspase cleavage site (Betin et al., 2012). A more positively charged targeting sequence has been found to enhance interaction with the mitochondrial membrane potential, facilitating import (Chacinska et al., 2009). Additionally, lengthening an MTS without changing its linear charge density has been shown to increase import (Wilcox et al., 2005). Thus, Su9 would be the preferred choice (Fig. S1E).

Mitochondrial import of the three versions of each CRISPR protein with either COX8A, Su9 or ATG4D MTS was tested. Each of the MTSs showed mitochondrial localisation by fluorescence microscopy as GFP fusion control constructs (data not shown). Using the compact SaCas9, targeting efficiency was clearly improved and mitochondria looked healthier, but relatively few cells showed mitochondria-targeted Cas9, and only a small proportion of the protein was localised to mitochondria (in most transfected cells, GFP was detected in the nucleus likely corresponding to mis-targeting Cas9 or free GFP) (Fig. 3A). However, in the case of LbCas12a or AsCas12a, using any of the MTSs, the protein was more reliably localised to mitochondria and the organelles looked healthy through fluorescence microscopy (Fig. 3A). In cells expressing COX8ALbCas12a or AsCas12a–GFP, some cytosolic signal was also observed, possibly due to protein mis-targeting. In contrast, when using Su9AsCas12a–GFP, Su9LbCas12a–GFP, ATG4DLbCas12a or ATG4DAsCas12a–GFP, almost all transfected cells showed mitochondrial targeting and healthy mitochondria (Fig. 3A). Mitochondrial colocalisation was confirmed by semiquantitative analysis of the images using fluorescence profiles of GFP and MitoTracker Red signals taken along a 150 px line (Fig. 3A), and by colocalisation analysis in ImageJ/Fiji (Fig. 3B). Further analysis of mitochondrial properties (density; branch length; MitoTracker intensity; Fig. 3C–E) revealed that none of the CRISPR effector/MTS combinations tested significantly altered mitochondrial properties within this

timescale. The absence of negative influence of MTS–SaCas9–GFP on mitochondrial parameters most likely reflects the relatively poor mitochondrial targeting of this effector as compared with SpyCas9 (see Fig. 2). A specific antibody was also used to confirm LbCas12a protein mitochondrial localisation in hTERT RPE1 cells transiently transfected with LbCas12a–GFP appended to either of the MTSs (Fig. 3F). Using immunoblotting, optimal expression was observed in lysates of RPE1 cells transfected with Su9LbCas12a–GFP (24 h post transfection) (Fig. 3G).

From our systematic tests, we can therefore conclude that LbCas12a traffics most efficiently to mitochondria, in particular using the Su9 MTS. Overall, our fluorescence data correlate with the bioinformatic predictions for the mitochondrial import of these CRISPR variants.

Assessment of LbCas12a-based MitoCRISPR activity in MELAS cybrid cells – considerations for tool development

To date, attempts at developing functional MitoCRISPR systems have measured changes in mtDNA copy number (Jo et al., 2015; Loutre et al., 2018; Orishchenko et al., 2016); however, a better way to validate targeted nuclease activity would be to demonstrate heteroplasmy purification, as seen, for example, with MitoTALENs (Hashimoto et al., 2015). In this study, we used cybrid cell line versions of a MELAS syndrome mutation as a possible model system to test the development of Cas12a-based MitoCRISPR tools. MELAS is one of the most common mitochondrial disorders. It is associated with neurological symptoms and other secondary manifestations, such as depression, cardiomyopathy and diabetes mellitus (Finsterer, 2004; Montagna et al., 1988; Sproule and Kaufmann, 2008). Although this syndrome can be caused by different mutations, 80% of patients harbour a transition of adenine to guanine at the 3243 position in the MT-TL1 gene [tRNALeu (UUR)] of mtDNA. This mutation leads to defects in mitochondrial protein synthesis and respiratory chain function (Chan, 2006; Liesa et al., 2009), and has the added practical advantage in this study of allowing rapid identification of WT and mutant mtDNA levels by PCR-restriction fragment length polymorphism (RFLP), as the mutation creates a novel restriction site for the enzyme ApaI (see Fig. S2A).

During our attempts to establish a working MitoCRISPR system using Su9LbCas12a–GFP with non-targeted and 5′RP crRNAs [based on previous reports of MitoCRISPR-type activity using non-targeted gRNAs (Jo et al., 2015; Orishchenko et al., 2016)], we encountered several practical difficulties that highlight the challenges of developing MitoCRISPR as a tool: (i) despite few obvious morphological changes, mitochondria in cell lines stably expressing Su9LbCas12a–GFP have reduced respiratory capacity (Fig. 4); (ii) as proteins are imported into mitochondria in their unfolded states, this precludes the use of assembled ribonuclear particles (Figs S3 and S4); (iii) the limited availability of suitable PAM sequences (a limitation of any CRISPR system, but particularly acute for heteroplasmy purification that must be targeted to specific mutations); (iv) the lack of specificity towards mutant versus WT mtDNA, due to inherent insensitivity of LbCas12a to mismatches (Fig. S5A,B); (v) inherent crRNA processing by LbCas12a, a feature that could prove useful for limiting the persistency of *in situ* CRISPR activity (Fig. S5C); (vi) poor reproducibility in functional MitoCRISPR assays (Fig. 5). In the following sections, we present our findings with respect to these limitations, along with attempts to demonstrate LbCas12a-mediated MitoCRISPR activity in cybrid cells.
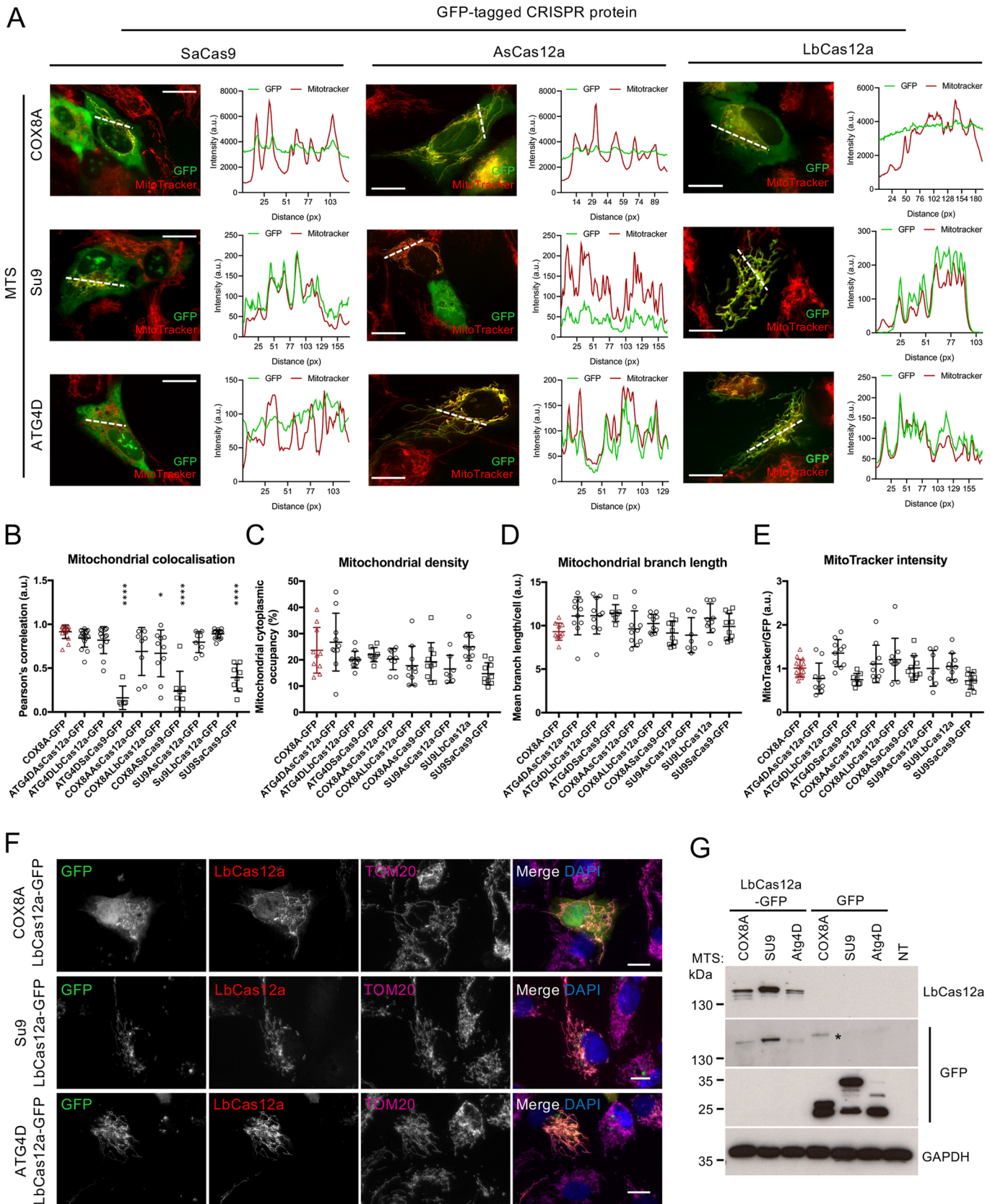
Fig. 3. See next page for legend.

Fig. 3. Su9LbCas12a–GFP showed the highest mitochondrial targeting efficiency and optimal expression levels in hTERT-immortalised human RPE1 cells. (A) Expression and localisation of LbCas12a–GFP, AsCas12a–GFP and SaCas9–GFP with various N-terminal MTSs in hTERT-immortalised human RPE1 cells. Example images and line scans (GFP and MitoTracker Red signals taken along the dashed 150 px line). (B–E) Analysis of mitochondrial parameters in RPE1 cells expressing MTS–Cas9 or MTS–Cas12a using different MTS types. (F) LbCas12a protein colocalises with mitochondria using any of the MTSs tested. Cells were transfected with the constructs shown, fixed, then stained with anti-Cas12a and anti-TOM20 antibodies. (G) Immunoblot of lysates of RPE1 cells transfected (24 h) with MTS–LbCas12a–GFP or MTS–GFP, using different MTSs. Lysates were probed for Cas12a, GFP (upper and lower gel range shown), and GAPDH (loading control). Optimal expression is observed in lysates of RPE1 cells transfected with Su9LbCas12a–GFP. A band was also detected in the COX8A-GFP sample fractionated by 8% SDS-PAGE (depicted by *), with a size that does not correspond to any of the constructs tested. Results are mean ±s.d.; *$P<0.05$; ****$P<0.0001$ (one-way ANOVA with Tukey's test). Scale bars: 10 μm. a.u., arbitrary units; NT, not transfected.

Mitochondrial targeting of Su9LbCas12a–GFP in cybrid cell lines for MitoCRISPR

Based on ApaI-mediated digestion, the heteroplasmy load of the cybrids used in this project was ∼100% for both WT and MELAS (Fig. S2A). Unfortunately, we were unable to source cybrid lines with intermediate heteroplasmy loads. Nonetheless, we consider that the ∼100% WT and MELAS cybrids still provide suitable controls to determine CRISPR activity and specificity. Su9LbCas12a–GFP and Su9–GFP were stably expressed in the cybrids by lentiviral infection followed by FACS sorting for high and low expressing populations (Fig. 4A,B; Fig. S2B–D). LbCa12a localisation to the mitochondrial matrix was confirmed by cell fractionation (Fig. 4C), TOM/TIM import blockers (Fig. S3) and immunoelectron microscopy (immunoEM) (Fig. 4D,E). In the cell fractionation experiments, mitochondria were isolated from WT cybrids transfected with Su9LbCas12a–GFP and treated with proteinase K to test whether mitochondria-targeted LbCas12a was protected from degradation (and therefore had been fully imported). Following the proteinase K treatment, both the mitochondrial matrix marker HSP60 (also known as HSPD1) and LbCas12a, but not the outer mitochondrial membrane (OMM) marker TOM20, were retained (Fig. 4C). Three LbCas12a bands were observed in the mitochondrial fraction using either polyclonal or monoclonal antibodies, likely comprising: (i) the precursor form; (ii) the mature protein; and (iii) a product likely corresponding to Su9LbCas12a separated from GFP (as this band was not detected with the antibody recognising GFP). Notably, the precursor:mature LbCas12a ratio changed following proteinase K treatment, such that only the precursor form was accessible and susceptible to degradation. WT cybrids stably expressing Su9LbCas12a–GFP were processed for immunoEM using anti-GFP (Fig. 4D) or anti-LbCas12a (Fig. 4E) primary antibodies, and 10 nm gold-conjugated secondary antibodies. A proportion of mitochondria had damaged or missing cristae in many of these cells (data not shown); however, focusing on mitochondria of healthy appearance, Su9LbCas12a–GFP was found to be localised to the mitochondrial matrix (Fig. 4D,E). Import of LbCas12a to the mitochondrial matrix through the TOM/TIM import route was confirmed by use of mitochondrial import blockers [MitoBloCK; MB-10 (a TIM23 inhibitor) or MB-12 (DECA; a TIM23 and ATP synthase inhibitor)] (Fig. S3). As expected, mis-localisation of the Su9LbCas12a fusion protein from mitochondria to the cytosol was observed in RPE1 cells (Fig. S3A) and WT/ MELAS cybrids (Fig. S3B,C) treated with 20 μM MB-10 or 10 μM MB-12 for 24 h.

The impact of LbCas12a mitochondrial import on mitochondrial respiration

The bioenergetic profile of cybrids stably expressing Su9LbCas12a–GFP was measured using the Seahorse XF Cell Mito Stress Test (Fig. 4F,G). As expected, WT cybrids, but not MELAS cybrids, showed normal mitochondrial respiration (oxygen consumption rate, OCR) profiles; however, OCR measured in WT cybrids stably expressing mitochondrial-localised LbCas12a at either low or high expression levels was significantly reduced (Fig. 4F). This was not observed with the control stable line expressing Su9–GFP (Fig. 4F). Against an already low baseline, mitochondrial respiration profiles were not further reduced in the MELAS cybrids stably expressing Su9LbCas12a–GFP (Fig. 4G). These data indicate that prolonged expression of Su9LbCas12a–GFP, although not adversely and grossly affecting mitochondrial morphology (Fig. 3), does impact on mitochondrial functionality at the level of mitochondrial respiration. We can therefore conclude that LbCas12a is localised to the matrix, as confirmed by cell fractionation or EM, but that mitochondrial respiration is affected in cybrids stably expressing Su9Cas12a–GFP. Whether this is due to exogenous protein overload and proteostasis stress, partial impairment of the protein import pathway due to the ongoing import of an unnatural mitochondrial protein, or Cas12a DNA-binding activity in the absence of crRNA is currently unclear.

Requirement for unfolding of LbCas12a during mitochondrial import

Any effective MitoCRISPR system would need to consider the mode of delivery of both CRISPR protein and gRNA/crRNA. In this study, we have focussed on expressing CRISPR proteins on plasmids and viral vectors. We also considered whether native CRISPR proteins appended with MTSs could be imported into mitochondria as pre-assembled RNPs for MitoCRISPR. Fig. S4A shows that import into isolated yeast mitochondria with recombinant Su9LbCas12a–Myc requires chemical denaturation, as no product is detected in proteinase K-treated samples using native protein (with or without intact proton motive force). To test for possible import of mitochondrial-targeted Cas12a post translation in living cells, we treated WT cybrids stably expressing Su9LbCas12a–GFP with MB-10 for 24 h (to block import), then washed out the drug and incubated cells for up to a further 16 h in the presence of cycloheximide (to block new protein expression). Although the bulk of the GFP signal remained cytosolic, a minor fraction of the protein produced before translation inhibition and after the release of the import block colocalised with TOM20-labelled mitochondria. This might be indicative of partial import of pre-folded Cas12a (Fig. S4B).

Analysis of mitochondrial LbCas12a cleavage activity and mtDNA levels in MELAS cybrids

We next tested whether expression of Su9LbCas12a with crRNAs could result in measurable changes in mtDNA, as has been suggested by previous studies. Since we used homoplasmic MELAS cybrids as the model system, a reduction in mtDNA copy number was expected following CRISPR nuclease activity inside mitochondria [mtDNA DSBs have been demonstrated to not be repaired, but rather the broken mtDNA is eliminated, probably by mitochondrial nucleases (Moretton et al., 2017)].

We designed Cas12a crRNAs specific for the MELAS mutation. Two different crRNAs were used to target the *MT-TL1* gene comprising the MELAS mutation (Fig. S5A). Each of them targeted a different DNA strand, and both were tested in untargeted or in mitochondrial-targeted formats. First, the DNA cleavage activity of
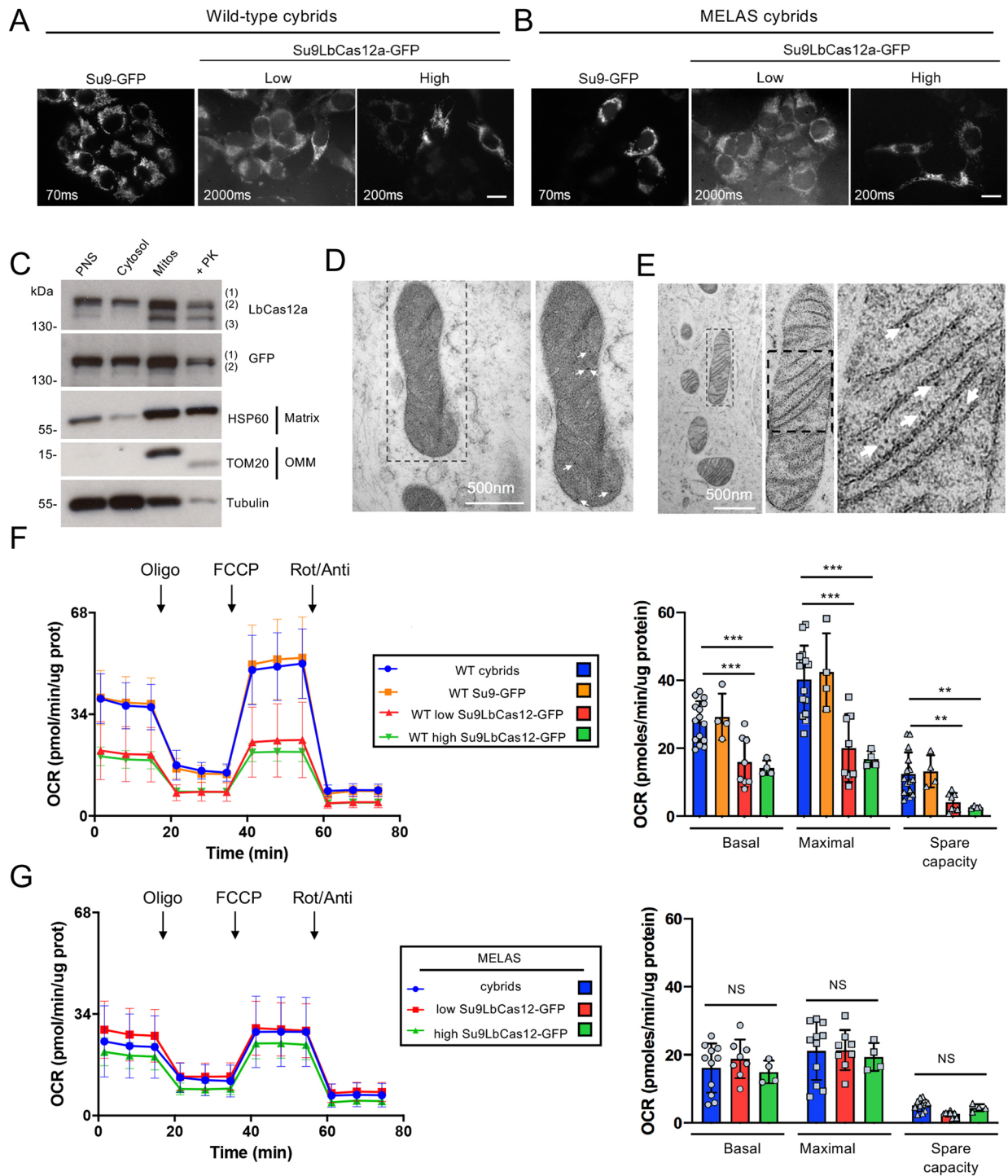
Fig. 4. MTS–Su9LbCas12a localises to the mitochondrial matrix in WT or MELAS cybrids, but reduces mitochondrial respiration. (A) WT and (B) MELAS cybrids stably expressing Su9–GFP or Su9LbCas12a–GFP with low or high expression levels. (C) Immunoblots of subcellular fractions of WT cybrids transiently expressing Su9LbCas12a–GFP. Immunoblots were carried out using a monoclonal anti-LbCas12a antibody, anti-GFP, mitochondrial markers (anti-HSP60 and anti-TOM20) and anti-tubulin. The positions of possible Su9LbCas12a–GFP species are indicated as follows: (1) full-length; (2) LbCas12a–GFP (i.e. with MTS removed); (3) (Su9)–LbCas12a (i.e. with GFP removed). PNS, post-nuclear supernatant; Mitos, mitochondrial fraction. (D,E) ImmunoEM images of mitochondria in WT cybrids stably expressing Su9LbCas12a–GFP stained with anti-GFP (D) or anti-LbCas12a (E) and 10 nm gold secondary antibodies. Arrows indicate gold particles. (F,G) Mitochondrial respiration profiles in (F) WT and (G) MELAS cybrids stably expressing Su9LbCas12a–GFP. Respiration parameters were measured using a XF Cell Mito Stress Test (Seahorse). Oligo, oligomycin; Rot/Anti, rotenone/antimycin A. Seahorse traces are shown to the left; oxygen consumption rate (OCR) data are shown to the right; $n=3$. Results are mean±s.d.; **$P<0.01$; ***$P<0.001$; NS, not significant vs control (Student's t-test). Scale bars: 10 μm.

LbCas12a using the four different crRNAs was assessed by cleavage assays *in vitro* (Fig. S5B). In these experiments, WT or mutant MT-TL1 DNA was cloned into a plasmid (pSP1), which was cut with a similar cleavage efficiency using any of the designed crRNAs. However, the cleavage appeared to be nonspecific as LbCas12a targeted both WT and mutant DNA containing the
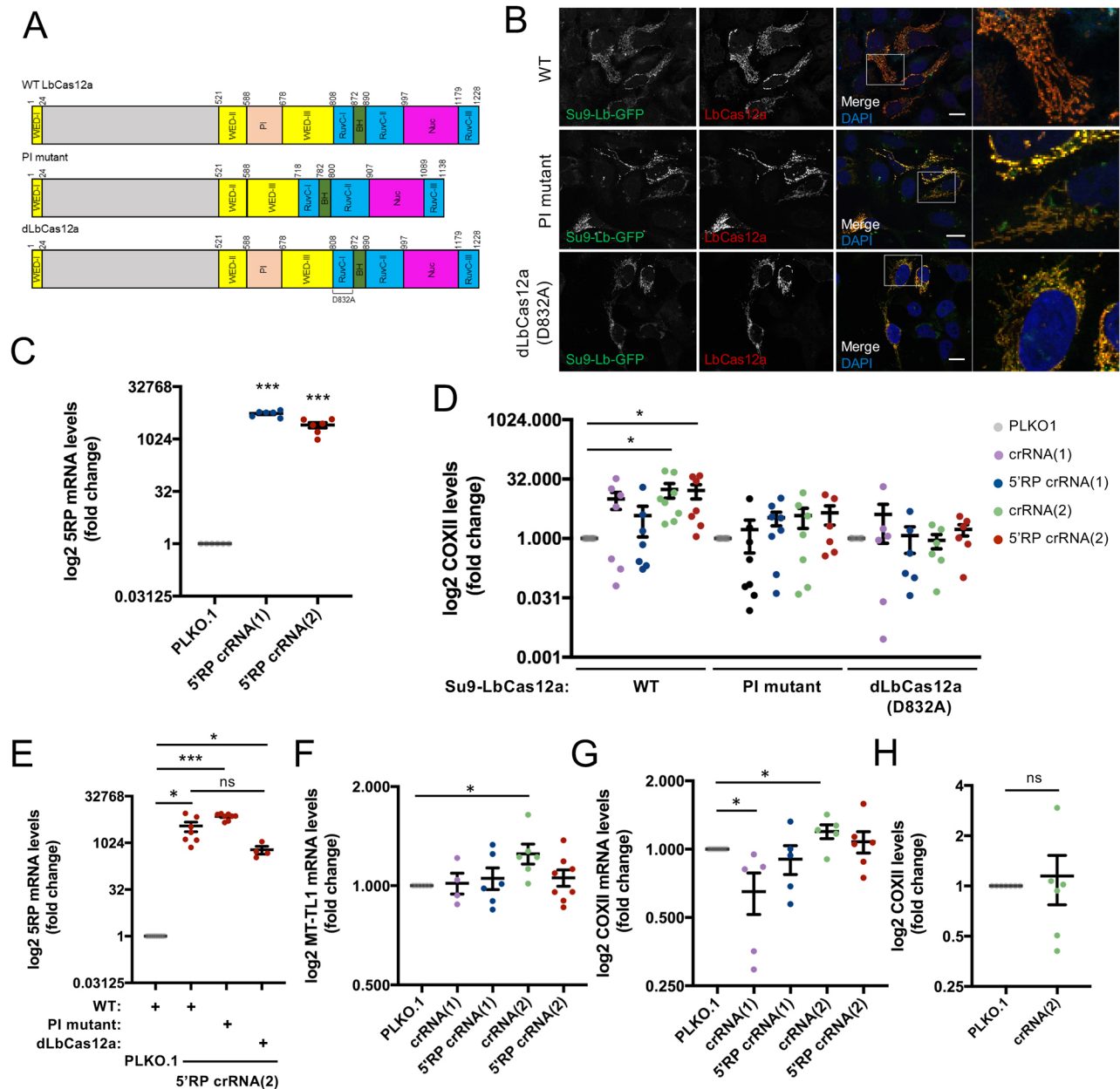
Fig. 5. Quantitative analysis of mitochondrial DNA and mRNA levels in MELAS cybrids following transient transfection of Su9LbCas12a–GFP. (A) Schematic diagram of the domain organization of WT LbCas12a, a PI mutant lacking the PAM-interacting (PI) domain, and the inactive form dLbCas12a (D832A). (B) Representative images showing expression and mitochondrial localisation of WT, PI mutant and dLbCas12a following co-transfection with PLKO.1 control in MELAS cybrids. (C) qRT-PCR analysis of 5′RP crRNA transcription in MELAS cybrids following PLKO.1, 5′RP crRNA(1) or 5′RP crRNA(2)/Su9LbCas12a-GFP co-transfections. (D) qPCR analysis of COXII DNA levels following PLKO.1, crRNA(1), 5′RP crRNA(1), crRNA(2), or 5′RP crRNA(2)/WT, PI mutant, or dLbCas12a co-transfections. (E) qRT-PCR analysis of 5′RP crRNA transcription in MELAS cybrids following 5′RP crRNA(2)/WT, PI mutant or dLbCas12a co-transfection as shown. (F,G) qRT-PCR analysis of MT-TL1 (F) and COXII (G) expression in MELAS cybrids following PLKO.1, crRNA(1), 5′RP crRNA(1), crRNA(2) or 5′RP crRNA(2) co-transfection with WT Su9LbCas12a-GFP. (H) qPCR analysis of COXII DNA levels following PLKO.1 or crRNA(2)/Su9LbCas12a-GFP co-transfection. Data was normalised to GAPDH. Results are means±s.e.m.; *$P<0.05$; ***$P<0.001$; ns, not significant vs PLKO.1 control (Student's t-test).

MELAS mutation (ApaI was used to distinguish the WT and mutant target sequences). The unspecific binding could be due to the insensitivity of Cas12a to mismatches at certain locations in the spacer (Swarts et al., 2017; Jones et al., 2019 preprint), or due to a recently reported lack of specificity of Cas12a under some conditions (Murugan et al., 2020). It should be noted that the cleavage activity is likely to be independent of a 5′ modification, since the 5′RP crRNA was found to be processed by LbCas12a *in vitro* (Fig. S5C). This feature of Cas12a is potentially useful since

a 5′ modification could be made to a crRNA to allow efficient import, and upon RNP assembly in the matrix, the crRNA would be processed so decreasing the likelihood of possible off-target effects.

Testing Su9LbCas12a–GFP for evidence of MitoCRISPR activity in MELAS cybrids

Despite its apparent lack of specificity, we decided to test the functionality of the Cas12a-crRNA system inside mitochondria. We compared three versions of LbCas12a: WT LbCas12a; a PAM

interacting (PI) domain mutant (PAM recognition is essential for initiation of R-loop formation); and a RuvC inactive version (dLbCas12a) containing the point mutation D832A, which is able to associate with DNA but not produce DNA breaks (Fig. 5A). For this test, we opted to use transient transfection of Cas12a proteins and crRNAs to avoid the functional decline observed in mitochondria over time in stable cell lines. Both WT and mutant forms of Su9LbCas12a–GFP localised strongly to mitochondria in MELAS cybrids co-transfected with a control (PLKO.1) plasmid (Fig. 5B). Next, mtDNA levels were analysed in MELAS cybrids transiently co-transfected (48 h) with unmodified crRNAs [crRNA(1) or crRNA(2)] or 5′RP crRNAs and mitochondria-targeted Su9LbCas12a–GFP (Fig. 5C–H). crRNA transcription was achieved by cloning the corresponding crRNA sequence into a PLKO.1 vector containing a U6 promoter.

Transcriptional activity of the transfected PLKO.1 plasmids was evaluated from crRNA levels using quantitative (q)RT-PCR in MELAS cybrids co-transfected with WT LbCas12a (Su9LbCas12a–GFP) (Fig. 5C). To evaluate mtDNA copy number, COXII DNA levels were measured by quantitative (q)PCR following a 48-h co-transfection of cybrids with WT or mutant Su9LbCas12a–GFP and the corresponding crRNA or empty PLKO.1 control vector (Fig. 5D). An unexpected increase in mtDNA levels was observed after transfection of MELAS cybrids with WT Su9LbCas12a–GFP and crRNA(2) or 5′RP crRNA(2). This effect was not observed using either of the mutant forms of Su9LbCas12a–GFP (non-DNA binding/non-cleavage) or using the crRNA(1)/5′RP(1) RNA versions (Fig. 5D), suggesting that both DNA binding and nuclease activity might be necessary to observe this effect. Similar crRNA transcription levels were observed using any of the protein variants after co-transfection of MELAS cybrids with 5′RP crRNA(2) and WT or mutant forms of Su9LbCas12a–GFP (Fig. 5E). This indicates that the lack of effect on mtDNA levels using mutant forms of Su9LbCas12a–GFP was not due to a lower crRNA transfection or transcription efficiency. Moreover, MT-TL1 and COXII mRNA levels also increased after co-transfection with WT Su9LbCas12a–GFP and crRNA(2) (Fig. 5F,G), although in this assay, we also recorded reduced COXII mRNA levels in cells co-transfected with WT Su9LbCas12a and crRNA(1) (Fig. 5G).

These data suggested that WT (active) Su9LbCas12a–GFP in conjunction with crRNA(2) (with or without mitochondrial targeting) elicits changes in mitochondria, resulting in elevated mtDNA levels. To being to understand the biology underpinning these changes, we carried out a further set of validation experiments to confirm the increase in COXII DNA levels after co-transfection with WT Su9LbCas12a–GFP and crRNA(2); however, no significant changes in mtDNA levels were observed (Fig. 5H). The reasons for this apparent variability in mitochondrial-targeted CRISPR/Cas12a system effects are currently unclear and will require further experimentation, including explicit demonstration of crRNA import into mitochondria and heteroplasmy purification using suitable cell lines.

DISCUSSION
Given the impact that technology for the efficient manipulation of mtDNA would have on the study of mtDNA and disease, it is not surprising that there have been several published efforts to develop MitoCRISPR techniques. However, none have yet described a tool that is as efficient as the best ZFN and TALEN examples. The most successful iteration to date has reported a depletion of mtDNA copy number (Loutre et al., 2018), but CRISPR-mediated heteroplasmy purification, the gold-standard for mtDNA editing, has yet to be

achieved. The work here aimed to provide a careful validation of MitoCRISPR toolkit parts.

Despite being used in all the previous studies, mitochondria-targeted SpyCas9 (COX8A–Cas9) showed poor mitochondrial localisation in transiently transfected mammalian cells as analysed by immunofluorescence. Moreover, cells expressing mitochondria-targeted SpyCas9 suffered a dramatic deterioration in mitochondrial morphology and function, which is likely to impact on cell viability. Overexpression and mitochondrial import of this large protein is likely to be disruptive to mitochondrial morphology/physiology. In contrast, LbCas12a was successfully expressed and localised to the mitochondrial matrix using several MTSs as measured by immunofluorescence, western blotting and immunoEM, with the most successful MTS being Su9. However, careful analysis of mitochondrial LbCas12a import and cellular impact using cell lines stably expressing Su9Cas12a–GFP showed evidence of mitochondrial damage caused by the prolonged expression of mitochondria-targeted LbCas12a. Therefore, if the mitochondria-targeted CRISPR/LbCas12a system were to be used further, transient expression would likely be needed to prevent mitochondrial disturbance. However, a more significant problem in using Cas12a is possible off-target cleavage activity. In contrast to the very reliable nuclease gene knockouts of classical CRISPR, heteroplasmy purification requires that the targeting occurs exactly at the mutated sequence. With the limitations of PAM availability, protospacer sequence choice could be limited to a single sequence. Consequently, if mismatches are tolerated by Cas12a, it will be difficult to achieve specificity.

The obvious difference in mitochondrial import efficiency observed for SpyCas9 and LbCas12a could be explained by various characteristics of the proteins overviewed in this work. The overall domain organisation of these enzymes is significantly different, particularly with respect to their N-terminal secondary structures, which are typically key for successful protein import into mitochondria. Furthermore, amino acid bias or differences in overall peptide charge of imported proteins also needs be considered, as favourable interactions with the TOM/TIM machinery will encourage mitochondrial import. This is consistent with LbCas12a being smaller, more positively charged and less hydrophobic than SpyCas9, which would also explain the higher mitochondria targeting efficiency shown for Cas12a. Moreover, MTS accessibility is important for protein import, and it may be that the peptide is suboptimally presented on Cas9. The use of alternative MTSs or introducing a flexible linker between the MTS and Cas9 structure in conjunction with directed in silico modelling, might ameliorate this. An appreciation of those features that favour Cas12a import over Cas9 could also be used to modify Cas9 structure, optimising it for mitochondrial import (for example, using a split Cas9; Wright et al., 2015). Alternatively, general rules governing mitochondrial import could be applied when screening the large number of CRISPR-Cas variants in the pangenome (Makarova et al., 2020). Alternative CRISPR-Cas enzyme may prove more efficient and less disruptive to organelle health. Ultimately, the standard empirical testing approach may prove to be the only way to reliably judge whether an effector protein–MTS combination will be useful.

Our data on RNA import add to other evidence for mitochondrial localisation of gRNAs without the requirement for targeting modifications (Gammage et al., 2018; Jo et al., 2015; Loutre et al., 2018). It should be noted that our assays do not explicitly demonstrate import, but rather RNase protection by membrane association and/or co-fractionation. Previous reports also suffer the same limitation. For protein import assays, evidence of delivery to

the matrix is ascertained by a change in protein size as the MTS is proteolytically removed (as seen in our *in vitro* Cas12a import assay; Fig. S4A). However, there are not any reports of an equivalent RNA aptamer processing activity in mitochondria to use as a functional readout. Further careful examination of mitochondrial compartments would be needed to prove whether the crRNA is matrix-located. A limitation of the aptamer-facilitated import of Cas9 gRNAs for mtDNA editing is that once bound to Cas9, 5′ modified gRNAs only support formation of small R-loops and completely block DNA cleavage (G.M. and M.D.S., unpublished observations). The processing of 5′ modifications by Cas12a removes any potential inhibition and is thus an additional advantage of the type V system over type II Cas9.

Data presented here indicate that in the presence of an active mitochondria-targeted Cas12a and crRNA, it is possible to observe an increase in the copy number of mtDNA. Changes in COXII and MT-TL1 mRNA levels were also recorded. Given that defects in mitochondria, such as dysfunctional mitochondrial dynamics or fragmentation, were not observed, the change in mtDNA copy number recorded might be due to a feedback mechanism triggered to (over)compensate for a perceived reduction in mtDNA. However, the lack of reproducibility in this assay currently remains the greatest hurdle in the application of MitoCRISPR. Given the non-ideal cybrid line available to us and lack of clear evidence for RNA import, we did not pursue the copy number experiments further. We would argue that any future studies need to demonstrate RNA import and to use heteroplasmy purification in the absence of significant changes in mitochondrial health as a benchmark for success, and that reproducibility and independent validation should be important goals. The recent breakthrough in base editing of mtDNA using DddA still relies on using TALEs (Mok et al., 2020). Progress in applying this technique could be accelerated if it could be linked to a more-easily programme endonuclease dead dCas effector. There is therefore still value in further developments to provide a working MitoCRISPR system.

MATERIALS AND METHODS
Reagents and antibodies
Unless stated otherwise, all reagents were from Sigma. Stock solutions of carbonyl cyanide m-chloro phenyl hydrazone (CCCP; C2759; 10 mM), DAPI (4′, 6-diamidino-2-phenylindole; D9542; 1 mg/ml), MB-10 (MCule; P-579567132), MB-12 (PHR1300-500MG), cycloheximide (TOKU-E, C084) and proteinase K (Thermo, EO0491; 10 mg/ml) were stored at −20°C. The following primary antibodies were used: anti-GAPDH [G8796; 1:2000 immunoblotting (IB)]; anti-GFP for IB (Covance, MMS-118R; 1:2000); anti-GFP for immunoEM (Rockland, 600-401-215; 1:250); anti-HSP60 [H4149; 1:2000 IB, 1:200 immunofluorescence (IF)]; anti-Tom20 (BD Biosciences, 612278; 1:750 IB, 1:75 IF); anti-tubulin (T5168; 1:2000 IB); polyclonal anti-LbCas12a (GeneTex, GTX133301; 1:1000 IB, 1:100 IF); monoclonal anti-LbCas12a (SAB4200777; 1:1000 IB). Anti-mouse HRP (Stratech, G32-62DC-SGC; 1:10,000); anti-rabbit-IgG conjugated to HRP (Stratech**,** G33-62G-SGC; 1:10,000); anti-mouse/rabbit-IgG conjugated to Alexa Fluor 488 (Invitrogen**,** A-11029/A-11034; 1:300 IF); anti-mouse/rabbit-IgG conjugated to Alexa Fluor 568 (Invitrogen, A-11031/A11036; 1:300 IF); anti-mouse/rabbit-IgG conjugated to Alexa Fluor 647 (Invitrogen, A-21236/A-21244; 1:300 IF). MitoTracker red CM-H_2Xros was from Thermo Fisher (M7513); VOA is 1 mM valinomycin, 10 mM oligomycin and 8 mM antimycin A.

Cell lines and cell culture
hTERT-immortilised human Retinal Pigment Epithelial (RPE1) cells (ATCC, ref. no. CRL-4000) were maintained in high-glucose DMEM (D5796) supplemented with 10% FBS (F7524) at 37°C in 5% CO_2. WT ACH cytoplasmic hybrid cells or 94αT3 MELAS cybrids carrying

m.A3243G mtDNA mutation (a kind gift from Dr José Sanchez-Alcázar, Seville, Spain; Garrido-Maraver et al., 2015)) were maintained in high-glucose DMEM supplemented with 5% FBS, 1 mM sodium pyruvate, 1% penicillin/streptomycin (P4333) and 50 µg/ml uridine at 37°C in 5% CO_2.

Plasmids and transfection
Transient transfections were performed with Lipofectamine 2000 Reagent (Thermo Scientific, 11668027) and OptiMEM reduced serum medium (Gibco) according to the manufacturer's instructions. The efficacy of cell transfection was checked using fluorescence microscopy. Plasmid sequences are available on request: pD1301-AD (DNA2.0) was used for expression of NLS–SpyCas9–GFP or COX8A–SpyCas9–GFP and unmodified Cas9 gRNA template generation; pEX-A2 (Eurofins) was used for 5′RP/5′FD gRNA template generation; pSP1 (Siksnys laboratory, Vilnius University, Lithuania; Szczelkun et al., 2014) was used as a plasmid cleavage assays substrate plasmid; pEGFP (Clontech) was used for expression of COX8A/ATG4D-(SaCas9/LbCas12a/AsCas12a)–GFP or LbCas12a–GFP; Su9-GFP (Addgene, #23214; Chen et al., 2003) was used for expression of Su9-(SaCas9/LbCas12a/AsCas12a/PI)-GFP and Su9-(mutant/dLbCas12a)-GFP; pLVX-puro (Clontech) was used for stable expression of Su9-(LbCas12a)-GFP; PLKO.1 (Addgene #10878; Moffat et al., 2006) was used for expression of Cas12a crRNAs; SaCas9, LbCas12a, AsCas12a, dLbCas12a [Addgene #61592 (Ran et al., 2015), #69988 (Zetsche et al., 2015), #69982 (Zetsche et al., 2015), #104563 (Tak et al., 2017)] were used for protein template generation.

Viruses, transduction and stable cell lines
Lentivirus were generated in HEK293T cells by transient transfection using PEI reagent. 27 µg of the plasmid of interest was transfected together with 20.4 µg of the packing plasmid pAX2 and 6.8 µg of the envelope plasmid pMGD2. Viruses were harvested 48 h after transfection. Medium was collected and centrifuged at 1500 ***g*** for 5 min and filtered with a 0.45 µm filter to remove cells and debris. Viruses were concentrated using Lenti-X Concentrator (Clontech). One volume of Lenti-X Concentrator was combined with three volumes of clarified supernatant. The mixture was incubated 1 h at 4°C, then centrifuged at 1500 ***g*** for 45 min at 4°C and the pellet resuspended in N2B27 medium or DMEM. For viral transduction, cybrids were plated in 6 cm dishes and transduced with the corresponding lentiviruses (7.5 µl/ml) in the presence of 8 µg/ml polybrene to increase transduction efficiency. After 2 days, GFP-positive cells were selected by fluorescence-activated cell sorting (FACS). The efficacy of stable line generation was checked using fluorescence microscopy.

Immunoblotting
Cells grown on 6-well plates were initially washed with ice-cold PBS, then lysed with 100–200 µl/well of ice-cold radioimmunoprecipitation assay (RIPA) buffer consisting of 50 mM Tris-HCl pH 7.4, 1% Triton X-100 (9002-93-1), 0.5% sodium deoxycholate (D6750), 150 mM NaCl (S9888), 0.1% SDS (436143) supplemented with one tablet of protease inhibitor per 10 ml of RIPA buffer. The homogenates were incubated on ice for 15 min, then cleared by centrifugation at 12,000 ***g*** for 15 min at 4°C. Supernatants were collected as soluble fractions. Proteins were transferred to nitrocellulose membranes (Biolabs, 1620115). Membranes were then incubated with primary antibody diluted in 5% milk or 2.5% BSA in Triton X-100 TBS buffer (T-TBS) overnight. Primary and secondary antibodies used are listed above. Membranes were then washed three times prior to incubation with ECL Chemiluminiscence reagents (Geneflow, K1-0170), and band intensities were detected in films (GE Healthcare, 28906837) using a film developer.

Subcellular fractionation and proteinase K treatment
Cybrid cells were plated on 10 cm dishes and transfected with the Su9LbCas12a–GFP construct using Lipofectamine 2000 for 48 h. Cells were trypsinised, washed in PBS and resuspended in mitochondrial import buffer (50 mM HEPES pH 7.1, 0.6 M sorbitol, 2 mM KH_2PO_4, 50 mM KCl, 10 mM $MgCl_2$ and protease inhibitors) (Vergnolle et al., 2005). Cells were lysed on ice using a ball bearing cell homogeniser (twenty passes at

10 μm clearance; Isobiotech, Heidelberg, Germany) then centrifuged at 800 g for 5 min to remove the heavy nuclear pellet. The postnuclear supernatant was then centrifuged for 15 min at 10,000 g, and the resulting mitochondria-containing pellet was washed with 140 μl import buffer and incubated in the absence or presence of 0.1 mg/ml proteinase K for 15 min on ice. The reaction was stopped by the addition of PMSF to 1 mM.

Immunofluorescence and microscopy
Cells were seeded on coverslips. Cells were washed twice with PBS and incubated with 4% formaldehyde for 15 min or −20°C methanol for 5 min. Cells were then incubated 30 min with primary antibody (listed above) in PBS. Cells were washed three times with PBS and incubated with the secondary antibodies (listed above) and counterstained with DAPI (Life Technologies, D121490, 100 ng/ml) for 10 min. Cells were then washed again with PBS and mounted in Mowiol. Fixed-cell images were obtained using an Olympus IX-71 inverted microscope (60× Uplan Fluorite objective; 0.65–1.25NA, oil immersion lens) fitted with a CoolSNAP HQ CCD camera (Photometrics, AZ) driven by MetaMorph software (Molecular Devices). Confocal microscopy was carried out using a Leica SP5-AOBS confocal laser scanning microscope (63×1.4NA oil immersion objective or 100×1.4 NA oil immersion objective) attached to a Leica DM I6000 inverted epifluorescence microscope. Laser lines were: 100 mW argon (for 458, 488, 514 nm excitation), 2 mW Orange HeNe (594 nm), and a 50 mW diode laser (405 nm). The microscope was run using Leica LAS AF software (Leica, Germany). Image analysis was performed using Fiji (National Institutes of Health, Bethesda, USA).

Analysis of DNA or cDNA levels by qRT-PCR
Cybrid cells were plated on 6 cm dishes (DNA) or 6-well plates (cDNA). Cells were transiently transfected with the corresponding constructs for 2 days. For DNA extraction, cells were then washed with ice-cold PBS and lysed with 200 μl lysis buffer (1% SDS, 10 mM EDTA and 50 mM Tris pH 8.1) and incubated on ice for 10 min. For the purification of DNA, the phenol-chloroform purification was used. Finally, the DNA pellet was resuspended in a final volume of 15 μl and diluted for qRT-PCR analysis with specific primers. For RNA extraction, after the corresponding transfection, cells were washed with PBS and then cells were lysed in 350 μl RLT buffer (Qiagen). Total RNA was extracted through columns using RNeasy kit (Qiagen, 74104) following manufacturer's instructions and genomic DNA was digested using DNaseI (Qiagen). RNA samples were reverse transcribed using High-Capacity RNA-to-cDNA™ Kit (Thermo Scientific, 4387406), according to manufacturer's protocol. The DNA or cDNA samples were amplified using SYBR Green (Life Technologies). The reaction was carried out using StepOnePlus System (Applied Biosystems) and the following conditions were selected: after an initial denaturation at 95°C for 10 min, 40 cycles with 95°C for 15 s (denaturation), 60°C for 30 s (annealing) and 60°C for 30 s (elongation). For the analysis, DNA or mRNA levels were estimated using the ΔΔCt method normalising data to GAPDH levels (Livak and Schmittgen, 2001).

Seahorse bioenergetics
Cybrid cells were plated according to manufacturer's instructions on 8-well Seahorse XFp plates (Agilent, 103010-100). The day of the assay, culture media was replaced with Seahorse XF base medium (Agilent) supplemented with 1 mM sodium pyruvate, 2 mM glutamine, and 10 mM glucose (pH 7.4) for 1 h at 37°C. The Mito Stress Test Kit (Agilent) was prepared according to the manufacturer's instructions: oligomycin (1 μM); carbonilcyanide ptriflouromethoxyphenylhydrazone (FCCP; 1 μM); rotenone/antimycin A (0.5 μM). After analysis, cells were lysed in 20 μl of RIPA buffer and protein levels were quantified by Nanodrop (A280) to normalise the data.

In vitro transcription of 33P-UTP-labelled RNA
In vitro transcription was performed using the T7 HiScribe High Yield RNA synthesis kit. The reaction was prepared to a final volume of 20 μl, containing a final concentration of 1× reaction buffer, 1 mM ATP, GTP and CTP. UTP was added to a final concentration of 4 μM with 0.25 μM α^{33}P-UTP, 0.5 MBq/reaction (Hartman Analytic, SRF 210). To this, 0.25 μg template DNA and 1 μl T7 RNA pol mix was added. The assembly was incubated at 37°C for 10 min, treated with DNase and purified with MicroBioSpin (BioRad) columns.

Denaturing urea-PAGE
RNA was separated on a denaturing urea-PAGE gel containing 10% (w/v) acrylamide, 1× Tris-borate EDTA (TBE) and 50% (w/v) urea. Gel mix was prepared, filter sterilised with a 0.2 μm nitrocellulose membrane and stored at 4°C for up to 2 weeks. Gels were set using the BioRad Mini-PROTEAN 3 system and pre-run in 1× TBE at 200 V for 45 min prior to loading samples. RNA samples were heated to 90°C with 1× RNA loading dye for 10 min and migrated in 1× TBE at 200 V. Gels were stained with 1 ml 1/1000 SYBR Gold Nucleic Acid Gel Stain (ThermoFisher Scientific) and imaged with the GelDoc™ XR+ system (BioRad).

CRISPR complex assembly and cleavage assay
250 nM *Lachnospiraceae bacterium* Cas12a protein was mixed with 250 nM crRNA in SB and incubated at 37°C for 1 h. For each cleavage reaction, 3 mM plasmid substrate (pSP1) was assembled in RB buffer at 37°C and preheated for 5 min. The reaction was started by addition of 50 nM assembled Cas12a CRISPR complex, which was incubated for the time period specified. The reaction was quenched by adding 80°C 3× STEB and incubating at 80°C for 5 min. Samples were separated by agarose gel electrophoresis on a 1.5% (w/v) agarose gel stained with ethidium bromide at 20 V overnight (16 h) and visualised by UV irradiation.

gRNA/crRNA sequences used
The following gRNA and crRNA sequences were used for Cas9 and Cas12a, respectively (shown in 5′–3′ orientation). Cas9 gRNA: GCGCU-AAAGAGGAAGAGGACAGUUUUAGAGCUAGAAAUAGCAAGUU-AAAAUAAGGCUAGUCCGUUAUCAACUUGAAAAAGUGGCACC-GAGUCGGUGCUUUUUU; Cas9 5′RP: GUCUCCCUGAGCUUC-AGGGAGCGCUAAAGAGGAAGAGGACAGUUUUAGAGCUAGA-AAUAGCAAGUUAAAAUAAGGCUAGUCCGUUAUCAACUUGA-AAAAGUGGCACCGAGUCGGUGCUUUUUU; Cas9 5′FD (F1D1): GGCGCAAUCGGUAGCGCUUCGAGCCCCCUACAGGGCUCCAC-CGCGCUAAAGAGGAAGAGGACAGUUUUAGAGCUAGAAAUA-GCAAGUUAAAAUAAGGCUAGUCCGUUAUCAACUUGAAAAA-GUGGCACCGAGUCGGUGCUUUUUU; Cas9 5′AD: GCCUUGUU-GGCGC-AAUCGGUAGCGCAAAUACAGGGCUCCACGCUAAAG-AGGAAGAGGACAGUUUUAGAGCUAGAAAUAGCAAGUUAAA-AUAAGGCUAGUCCGUUAUCAACUUGAAAAAGUGGCACCGAG-UCGGUGCUUUUUU; Cas12a crRNA (1): AAUUUCUACUAAG-UGUAGAUUUAAGAUGGCAGGGCCCGGUAAUC; Cas12a crRNA (2): AUUUCUACUAAGUGUAGAUUGCGAUUACCGGGCCCUGC-CAUCU.

Isolation of yeast mitochondria
Yeast (YPH499) were grown in 400 ml YPG with Pen/Strep at 24°C, 150 rpm for ~48-72 h. When OD600=7.5, cells were sub-cultured into 2×1 liters YPG pH 5.2 supplemented with Pen/Strep to OD600=0.5, then grown overnight at 19°C, 120 rpm. When OD600=1.2-1.8, cells were pelleted (4000 g, 10 min, RT) and pellets re-suspended in dH$_2$O. Mitochondria were isolated through differential centrifugation after cell wall was reduced by DTT as described in (Pereira et al., 2019).The final mitochondrial pellet was resuspended in 250 mM sucrose and 10 mM MOPS, pH 7.2. Mitochondrial protein was quantified by BCA assay, using BSA as standard. 1 mg aliquots were snap frozen and stored at −80°C.

Import of radiolabelled RNA into isolated yeast mitochondria
Isolated yeast mitochondria were thawed on ice and diluted in ice-cold yeast import buffer (50 mM sucrose, 80 mM KCl, 5 mM MgCl$_2$, 10 mM KH$_2$PO$_4$/K$_2$HPO$_4$ pH 7.2, 10 mM MOPS) with 2 mM ATP and 2 mM NADH added just before use. 100 μg mitochondria were diluted into 100 μl import buffer per condition. The mitochondrial suspension was preheated to 25°C in a thermo-mixer with gentle shaking and import started by addition

of ^{33}P-labelled RNA, gentle vortex and incubation at 25°C. Import was stopped after 5 min with VOA. The sample was split into two Eppendorf tubes (50 µl each) and one tube incubated with 5 µg RNase A for 15 min at 25°C. RNase was stopped with 1.5 µl RNase inhibitor and incubated for 10 min at 25°C, then washed twice with 250 µl yeast import buffer with 1 µl RNase inhibitor. Samples were centrifuged at 17,000 g for 10 min, and washed pellets either run on a denaturing urea-PAGE gel directly, or the RNA extracted with TRIzol reagent. For TRIzol extraction of RNA, each pellet was resuspended in 250 µl TRIzol reagent and tubes were incubated at room temperature for 5 min, 50 µl chloroform was added and tubes incubated for a further 5 min at room temperature. Samples were centrigued for 15 min at 12,000 g and 4°C, and the upper aqueous phase transferred to a new tube with 125 µl isopropanol with 0.05 µg/µl glycogen and incubated for 10 min at room temperature. Precipitated RNA was pelleted by centrifugation at 12,000 g for 10 min, 4°C, and pelleted RNA was washed twice with 250 µl 75% (v/v) ethanol (7500 g, 5 min, 4°C), air dried and resuspended in 10 µl 2× formamide RNA-loading buffer. For direct separation by denaturing-PAGE electrophoresis, pellets were resuspended in 5 µl yeast import buffer and 5 µl 2× formamide RNA-loading buffer. RNA in formamide RNA loading buffer was heated to 100°C for 10 min before separation by denaturing urea-PAGE. The gel was fixed with in-gel fixing solution [10% (v/v) methanol, 10% (v/v) acetic acid] for 1 h, then 30 min gel fixing solution with 5% (v/v) glycerol. The gel was dried with a pre-programmed schedule (up to 80°C, over 2 h) on a BioRad model 583 gel dryer, and then exposed on a phosphorimager screen (Fujifilm). The phosphor screen was imaged with a Typhoon-Trio scanner (GE Healthcare).

Cellular fractionation and isolation of RNA for northern blotting
HeLa cells were seeded to be 90% confluent on the day of the fractionation. Medium was aspirated, and cells were washed twice with PBS. Cells were detached with trypsin and transferred into a 15 ml falcon tube and centrifuged at 600 g at 4°C for 10 min. The cell pellet was resuspended in 1 ml ice-cold isolation buffer [0.44 M sorbitol, 40 mM EDTA, 10 mM HEPES-NaOH (pH 6.7), 0.1% (w/v) SDS]. Cells were homogenised using a cell homogeniser with an 8 µm spacing ball bearing, according to the manufacturer's instructions. 100 µl of whole-cell extract was kept for later RNA extraction. The remaining homogenate was centrifuged at 1500 g for 5 min at 4°C to pellet nuclei. The mitochondria-containing supernatant was collected and centrifuged at 15,000 g for 20 min at 4°C to pellet mitochondria. The supernatant, representing the cytosolic fraction, was kept on ice and the pellet was washed with isolation buffer and resuspended in 300 µl isolation buffer prior to disruption of the outer mitochondrial membrane with 60 ng/µl digitonin for 7 min at room temperature. Digitonin was diluted by a wash with 700 µl isolation buffer, and after a final wash the mitochondrial pellet, nuclear pellet, cytoplasmic fraction and whole-cell sample were resuspended in 500 µl TRIzol and stored at −80°C prior to RNA extraction as per the manufacturer's instructions.

Northern blotting
Urea-PAGE gels containing separated RNAs were electro-transferred onto Hybond XL nylon membrane (GE Healthcare) at 12 V over 12 h in 0.5× TBE for northern hybridisation. RNAs were fixed onto nylon membrane by UV irradiation at 1500×100 µJ/cm^2. Membranes were prehybridised in 6× SSC, 0.1% (w/v) SDS, 10× Denhardt's solution for 1 h at 65°C. 20× SSC [3 M NaCl, 0.3 M sodium citrate, 1 mM EDTA; 100× Denhardt's [2% (w/v) BSA, 2% (w/v) Ficoll 400, 2% (w/v) polyvinylpyrrolidone]. Hybridisation of 8×7 cm membranes in 50 ml falcons used 2.9 ml prehybridisation solution. Membranes were hybridised in one volume of prehybridisation solution containing one volume ([probe]$_f$: 2 ng/ml) 5′-^{32}P-labelled oligonucleotide probe by incubation overnight at 5°C. Probes of known cytoplasmic and mitochondrial RNAs were used as positive controls for cellular compartments, and designed hybridisation probes against gRNAs and mitochondrial targeted RNA aptamers determined transfected RNA cellular localisation. Following hybridisation, membranes were washed three times for 10 min in 2× SSC and 0.1% (w/v) SDS at room temperature and exposed on a phosphorimager screen which was imaged with a Typhoon-Trio scanner (GE Healthcare). The following primers/oligonucleotides were used [5′–3′ (length)]: Cyto tRNA$^{Lys}_{UUU}$ hybridisation

probe, ACTTGAACCCTGGACC (16); Mito tRNA^{Leu} hybridisation probe, GAACCTCTGACTCTAAAG (18); Mito tRNA^{Thr} hybridisation probe, TCTCCGGTTTACAAGAC (17); tRK1 hybridisation probe: TGGAGCC-CTGTAGGGG (16); and gRNA hybridisation probe, GCACCGACTCG-GTGCCACTT (20).

Labelling hybridisation probes
Dephosphorylated DNA oligonucleotides were labelled with bacteriophage T4 polynucleotide kinase by incubation for 1 h at 37°C with a 5-fold molar excess of 10 mCi/ml γ-^{32}P-ATP (Hartman Analytic, SRP 301) as per the manufacturers' instructions. The reaction was terminated by addition of EDTA (final concentration 20 mM), and probes were purified from unincorporated nucleotide with BioRad Micro Bio Spin P-6 columns.

Statistics
Graphical results were analysed with GraphPad Prism 7 (GraftPad Software, San Diego, CA), using an unpaired Student's t-test or one-way ANOVA, as indicated. *$P<0.05$, **$P<0.01$ and ***$P<0.001$. Results are expressed as mean±s.e.m. or mean±s.d., as indicated.

Author contributions
Conceptualization: M.v.d.K., M.D.S., J.D.L.; Methodology: Z.A., G.M., H.C.F., M.v.d.K., M.D.S., J.D.L.; Validation: M.D.S., J.D.L.; Formal analysis: Z.A., G.M., M.v.d.K., M.D.S., J.D.L.; Investigation: Z.A., G.M., H.C.F., M.D.S.; Resources: M.D.S., J.D.L.; Writing - original draft: Z.A.; Writing - review & editing: Z.A., H.C.F., M.D.S., J.D.L.; Visualization: Z.A., M.D.S., J.D.L.; Supervision: M.D.S., J.D.L.; Project administration: M.D.S., J.D.L.; Funding acquisition: M.D.S., J.D.L.

Supplementary information
Supplementary information available online at
https://jcs.biologists.org/lookup/doi/10.1242/jcs.248468.supplemental

Peer review history
The peer review history is available online at
https://jcs.biologists.org/lookup/doi/10.1242/jcs.248468.reviewer-comments.pdf

References
Bayona-Bafaluy, M. P., Blits, B., Battersby, B. J., Shoubridge, E. A. and Moraes, C. T. (2005). Rapid directional shift of mitochondrial DNA heteroplasmy in animal tissues by a mitochondrially targeted restriction endonuclease. *Proc. Natl. Acad. Sci. USA* **102**, 14392-14397. doi:10.1073/pnas.0502896102

Betin, V. M. S., MacVicar, T. D. B., Parsons, S. F., Anstee, D. J. and Lane, J. D. (2012). A cryptic mitochondrial targeting motif in Atg4D links caspase cleavage with mitochondrial import and oxidative stress. *Autophagy* **8**, 664-676. doi:10.4161/auto.19227

Bogdanove, A. J., Bohm, A., Miller, J. C., Morgan, R. D. and Stoddard, B. L. (2018). Engineering altered protein-DNA recognition specificity. *Nucleic Acids Res.* **46**, 4845-4871. doi:10.1093/nar/gky289

Chacinska, A., Koehler, C. M., Milenkovic, D., Lithgow, T. and Pfanner, N. (2009). Importing mitochondrial proteins: machineries and mechanisms. *Cell* **138**, 628-644. doi:10.1016/j.cell.2009.08.005

Chan, D. C. (2006). Mitochondrial fusion and fission in mammals. *Annu. Rev. Cell Dev. Biol.* **22**, 79-99. doi:10.1146/annurev.cellbio.22.010305.104638

Chen, H., Detmer, S. A., Ewald, A. J., Griffin, E. E., Fraser, S. E. and Chan, D. C. (2003). Mitofusins Mfn1 and Mfn2 coordinately regulate mitochondrial fusion and are essential for embryonic development. *J. Cell Biol.* **160**, 189-200. doi:10.1083/jcb.200211046

Chicani, C. F., Chu, E. R., Miller, G., Kelman, S. E. and Sadun, A. A. (2013). Comparing EPI-743 treatment in siblings with Leber's hereditary optic neuropathy mt14484 mutation. *Can. J. Ophthalmol.* **48**, e130-e133. doi:10.1016/j.jcjo.2013.05.011

Comte, C., Tonin, Y., Heckel-Mager, A.-M., Boucheham, A., Smirnov, A., Auré, K., Lombès, A., Martin, R. P., Entelis, N. and Tarassov, I. (2013). Mitochondrial targeting of recombinant RNAs modulates the level of a heteroplasmic mutation in human mitochondrial DNA associated with Kearns Sayre Syndrome. *Nucleic Acids Res.* **41**, 418-433. doi:10.1093/nar/gks965

DiMauro, S. and Hirano, M. (2009). Pathogenesis and treatment of mitochondrial disorders. *Adv. Exp. Med. Biol.* **652**, 139-170. doi:10.1007/978-90-481-2813-6_10

DiMauro, S. and Schon, E. A. (2003). Mitochondrial respiratory-chain diseases. *N. Engl. J. Med.* **348**, 2656-2668. doi:10.1056/NEJMra022567

Dovydenko, I., Heckel, A.-M., Tonin, Y., Gowher, A., Venyaminova, A., Tarassov, I. and Entelis, N. (2015). Mitochondrial targeting of recombinant RNA. *Methods Mol. Biol.* **1265**, 209-225. doi:10.1007/978-1-4939-2288-8_16

Entelis, N., Brandina, I., Kamenski, P., Krasheninnikov, I. A., Martin, R. P. and Tarassov, I. (2006). A glycolytic enzyme, enolase, is recruited as a cofactor of tRNA targeting toward mitochondria in Saccharomyces cerevisiae. *Genes Dev.* **20**, 1609-1620. doi:10.1101/gad.385706

Finsterer, J. (2004). Mitochondriopathies. *Eur. J. Neurol.* **11**, 163-186. doi:10.1046/j.1351-5101.2003.00728.x

Fukasawa, Y., Tsuji, J., Fu, S.-C., Tomii, K., Horton, P. and Imai, K. (2015). MitoFates: improved prediction of mitochondrial targeting sequences and their cleavage sites. *Mol. Cell. Proteomics* **14**, 1113-1126. doi:10.1074/mcp.M114.043083

Gammage, P. A., Moraes, C. T. and Minczuk, M. (2018). Mitochondrial genome engineering: the revolution may not be CRISPR-Ized. *Trends Genet.* **34**, 101-110. doi:10.1016/j.tig.2017.11.001

Garrido-Maraver, J., Paz, M. V., Cordero, M. D., Bautista-Lorite, J., Oropesa-Ávila, M., de la Mata, M., Pavón, A. D., de Lavera, I., Alcocer-Gómez, E., Galán, F. et al. (2015). Critical role of AMP-activated protein kinase in the balance between mitophagy and mitochondrial biogenesis in MELAS disease. *Biochim. Biophys. Acta* **1852**, 2535-2553. doi:10.1016/j.bbadis.2015.08.027

Hartl, F.-U., Pfanner, N., Nicholson, D. W. and Neupert, W. (1989). Mitochondrial protein import. *Biochim. Biophys. Acta* **988**, 1-45. doi:10.1016/0304-4157(89)90002-6

Hashimoto, M., Bacman, S. R., Peralta, S., Falk, M. J., Chomyn, A., Chan, D. C., Williams, S. L. and Moraes, C. T. (2015). MitoTALEN: a general approach to reduce mutant mtDNA loads and restore oxidative phosphorylation function in mitochondrial diseases. *Mol. Ther.* **23**, 1592-1599. doi:10.1038/mt.2015.126

Holzmann, J., Frank, P., Löffler, E., Bennett, K. L., Gerner, C. and Rossmanith, W. (2008). RNase P without RNA: identification and functional reconstitution of the human mitochondrial tRNA processing enzyme. *Cell* **135**, 462-474. doi:10.1016/j.cell.2008.09.013

Jinek, M., Chylinski, K., Fonfara, I., Hauer, M., Doudna, J. A. and Charpentier, E. (2012). A programmable dual-RNA-guided DNA endonuclease in adaptive bacterial immunity. *Science* **337**, 816-821. doi:10.1126/science.1225829

Jo, A., Ham, S., Lee, G. H., Lee, Y.-I., Kim, S., Lee, Y.-S., Shin, J.-H. and Lee, Y. (2015). Efficient Mitochondrial Genome Editing by CRISPR/Cas9. *Biomed Res Int* **2015**, 305716. doi:10.1155/2015/305716

Jones Jr, S. K., Hawkins, J. A., Johnson, N. V. Jung, C., Hu, K., Rybarski, J. R., Chen, J. S., Doudna, J. A. Press, W. H. and Finkelstein, I. J. (2019).Massively parallel kinetic profiling of natural and engineered CRISPR nucleases. *bioRxiv*, 696393 doi: https://doi.org/10.1101/696393

Kamenski, P., Smirnova, E., Kolesnikova, O., Krasheninnikov, I. A., Martin, R. P., Entelis, N. and Tarassov, I. (2010). tRNA mitochondrial import in yeast: Mapping of the import determinants in the carrier protein, the precursor of mitochondrial lysyl-tRNA synthetase. *Mitochondrion* **10**, 284-293. doi:10.1016/j.mito.2010.01.002

Kolesnikova, O., Kazakova, H., Comte, C., Steinberg, S., Kamenski, P., Martin, R. P., Tarassov, I. and Entelis, N. (2010). Selection of RNA aptamers imported into yeast and human mitochondria. *RNA* **16**, 926-941. doi:10.1261/rna.1914110

Liesa, M., Palacín, M. and Zorzano, A. (2009). Mitochondrial dynamics in mammalian health and disease. *Physiol. Rev.* **89**, 799-845. doi:10.1152/physrev.00030.2008

Livak, K. J. and Schmittgen, T. D. (2001). Analysis of relative gene expression data using real-time quantitative PCR and the $2-\Delta\Delta CT$ Method. *Methods* **25**, 402-408. doi:10.1006/meth.2001.1262

Loutre, R., Heckel, A.-M., Smirnova, A., Entelis, N. and Tarassov, I. (2018). Can Mitochondrial DNA be CRISPRized: Pro and Contra. *IUBMB Life* **70**, 1233-1239. doi:10.1002/iub.1919

Magalhães, P. J., Andreu, A. L. and Schon, E. A. (1998). Evidence for the presence of 5S rRNA in mammalian mitochondria. *Mol. Biol. Cell* **9**, 2375-2382. doi:10.1091/mbc.9.9.2375

Makarova, K. S., Wolf, Y. I., Iranzo, J., Shmakov, S. A., Alkhnbashi, O. S., Brouns, S. J. J., Charpentier, E., Cheng, D., Haft, D. H., Horvath, P. et al.

(2020). Evolutionary classification of CRISPR-Cas systems: a burst of class 2 and derived variants. *Nat. Rev. Microbiol.* **18**, 67-83. doi:10.1038/s41579-019-0299-x

Mercer, T. R., Neph, S., Dinger, M. E., Crawford, J., Smith, M. A., Shearwood, A.-M. J., Haugen, E., Bracken, C. P., Rackham, O., Stamatoyannopoulos, J. A. et al. (2011). The human mitochondrial transcriptome. *Cell* **146**, 645-658. doi:10.1016/j.cell.2011.06.051

Minczuk, M., Papworth, M. A., Kolasinska, P., Murphy, M. P. and Klug, A. (2006). Sequence-specific modification of mitochondrial DNA using a chimeric zinc finger methylase. *Proc. Natl. Acad. Sci. USA* **103**, 19689-19694. doi:10.1073/pnas.0609502103

Moffat, J., Grueneberg, D. A., Yang, X., Kim, S. Y., Kloepfer, A. M., Hinkle, G., Piqani, B., Eisenhaure, T. M., Luo, B., Grenier, J. K. et al. (2006). A lentiviral RNAi library for human and mouse genes applied to an arrayed viral high-content screen. *Cell* **124**, 1283-1298. doi:10.1016/j.cell.2006.01.040

Mojica, F. J. M., Díez-Villaseñor, C., García-Martínez, J. and Almendros, C. (2009). Short motif sequences determine the targets of the prokaryotic CRISPR defence system. *Microbiology* **155**, 733-740. doi:10.1099/mic.0.023960-0

Mok, B. Y., de Moraes, M. H., Zeng, J., Bosch, D. E., Kotrys, A. V., Raguram, A., Hsu, F., Radey, M. C., Peterson, S. B., Mootha, V. K. et al. (2020). A bacterial cytidine deaminase toxin enables CRISPR-free mitochondrial base editing. *Nature* **583**, 631-637. doi:10.1038/s41586-020-2477-4

Montagna, P., Gallassi, R., Medori, R., Govoni, E., Zeviani, M., Di Mauro, S., Lugaresi, E. and Andermann, F. (1988). MELAS syndrome: characteristic migrainous and epileptic features and maternal transmission. *Neurology* **38**, 751-754. doi:10.1212/WNL.38.5.751

Moraes, C. T., Bacman, S. R. and Williams, S. L. (2014). Manipulating mitochondrial genomes in the clinic: playing by different rules. *Trends Cell Biol.* **24**, 209-211. doi:10.1016/j.tcb.2014.02.002

Moretton, A., Morel, F., Macao, B., Lachaume, P., Ishak, L., Lefebvre, M., Garreau-Balandier, I., Vernet, P., Falkenberg, M. and Farge, G. (2017). Selective mitochondrial DNA degradation following double-strand breaks. *PLoS ONE* **12**, e0176795. doi:10.1371/journal.pone.0176795

Murugan, K., Seetharam, A. S., Severin, A. J. and Sashital, D. G. (2020). CRISPR-Cas12a has widespread off-target and dsDNA-nicking effects. *J. Biol. Chem.* **295**, 5538-5553. doi:10.1074/jbc.RA120.012933

Niazi, A. K., Mileshina, D., Cosset, A., Val, R., Weber-Lotfi, F. and Dietrich, A. (2013). Targeting nucleic acids into mitochondria: progress and prospects. *Mitochondrion* **13**, 548-558. doi:10.1016/j.mito.2012.05.004

Orishchenko, K. E., Sofronova, J. K., Chupakhin, E. G. and Lunev, E. A. and Mazunin, I. O. (2016). Import of Cas9 nuclease in mitochondria [in Russian]. *Genes Cells* **11**, 100-105.

Patananan, A. N., Wu, T.-H., Chiou, P.-Y. and Teitell, M. A. (2016). Modifying the mitochondrial genome. *Cell Metab.* **23**, 785-796. doi:10.1016/j.cmet.2016.04.004

Peeva, V., Blei, D., Trombly, G., Corsi, S., Szukszto, M. J., Rebelo-Guiomar, P., Gammage, P. A., Kudin, A. P., Becker, C., Altmüller, J. et al. (2018). Linear mitochondrial DNA is rapidly degraded by components of the replication machinery. *Nat. Commun.* **9**, 1727. doi:10.1038/s41467-018-04131-w

Pereira, C. V. and Moraes, C. T. (2017). Current strategies towards therapeutic manipulation of mtDNA heteroplasmy. *Front. Biosci. (Landmark Ed)* **22**, 991-1010. doi:10.2741/4529

Pereira, G. C., Allen, W. J., Watkins, D. W., Buddrus, L., Noone, D., Liu, X., Richardson, A. P., Chacinska, A. and Collinson, I. (2019). A high-resolution luminescent assay for rapid and continuous monitoring of protein translocation across biological membranes. *J. Mol. Biol.* **431**, 1689-1699. doi:10.1016/j.jmb.2019.03.007

Phillips, A. F., Millet, A. R., Tigano, M., Dubois, S. M., Crimmins, H., Babin, L., Charpentier, M., Piganeau, M., Brunet, E. and Sfeir, A. (2017). Single-molecule analysis of mtDNA replication uncovers the basis of the common deletion. *Mol. Cell* **65**, 527-538.e6. doi:10.1016/j.molcel.2016.12.014

Puranam, R. S. and Attardi, G. (2001). The RNase P associated with HeLa cell mitochondria contains an essential RNA component identical in sequence to that of the nuclear RNase P. *Mol. Cell. Biol.* **21**, 548-561. doi:10.1128/MCB.21.2.548-561.2001

Rahman, J. and Rahman, S. (2018). Mitochondrial medicine in the omics era. *Lancet* **391**, 2560-2574. doi:10.1016/S0140-6736(18)30727-X

Ran, F. A., Cong, L., Yan, W. X., Scott, D. A., Gootenberg, J. S., Kriz, A. J., Zetsche, B., Shalem, O., Wu, X., Makarova, K. S. et al. (2015). In vivo genome editing using Staphylococcus aureus Cas9. *Nature* **520**, 186-191. doi:10.1038/nature14299

Smirnov, A., Tarassov, I., Mager-Heckel, A.-M., Letzelter, M., Martin, R. P., Krasheninnikov, I. A. and Entelis, N. (2008). Two distinct structural elements of 5S rRNA are needed for its import into human mitochondria. *RNA* **14**, 749-759. doi:10.1261/rna.952208

Smirnov, A., Comte, C., Mager-Heckel, A.-M., Addis, V., Krasheninnikov, I. A., Martin, R. P., Entelis, N. and Tarassov, I. (2010). Mitochondrial enzyme rhodanese is essential for 5 S ribosomal RNA import into human mitochondria. *J. Biol. Chem.* **285**, 30792-30803. doi:10.1074/jbc.M110.151183

Sproule, D. M. and Kaufmann, P. (2008). Mitochondrial encephalopathy, lactic acidosis, and strokelike episodes: basic concepts, clinical phenotype, and

therapeutic management of MELAS syndrome. *Ann. N. Y. Acad. Sci.* **1142**, 133-158. doi:10.1196/annals.1444.011

Sripada, L., Tomar, D., Prajapati, P., Singh, R., Singh, A. K. and Singh, R. (2012). Systematic analysis of small RNAs associated with human mitochondria by deep sequencing: detailed analysis of mitochondrial associated miRNA. *PLoS ONE* **7**, e44873. doi:10.1371/journal.pone.0044873

Srivastava, S. and Moraes, C. T. (2001). Manipulating mitochondrial DNA heteroplasmy by a mitochondrially targeted restriction endonuclease. *Hum. Mol. Genet.* **10**, 3093-3099. doi:10.1093/hmg/10.26.3093

Sternberg, S. H. and Doudna, J. A. (2015). Expanding the biologist's toolkit with CRISPR-Cas9. *Mol. Cell* **58**, 568-574. doi:10.1016/j.molcel.2015.02.032

Swarts, D. C. (2019). Making the cut(s): how Cas12a cleaves target and non-target DNA. *Biochem. Soc. Trans.* **47**, 1499-1510. doi:10.1042/BST20190564

Swarts, D. C., van der Oost, J. and Jinek, M. (2017). Structural basis for guide RNA processing and seed-dependent DNA targeting by CRISPR-Cas12a. *Mol. Cell* **66**, 221-233.e4. doi:10.1016/j.molcel.2017.03.016

Szczelkun, M. D., Tikhomirova, M. S., Sinkunas, T., Gasiunas, G., Karvelis, T., Pschera, P., Siksnys, V. and Seidel, R. (2014). Direct observation of R-loop formation by single RNA-guided Cas9 and Cascade effector complexes. *Proc. Natl. Acad. Sci. USA* **111**, 9798-9803. doi:10.1073/pnas.1402597111

Tak, Y. E., Kleinstiver, B. P., Nuñez, J. K., Hsu, J. Y., Horng, J. E., Gong, J., Weissman, J. S. and Joung, J. K. (2017). Inducible and multiplex gene regulation using CRISPR-Cpf1-based transcription factors. *Nat. Methods* **14**, 1163-1166. doi:10.1038/nmeth.4483

Verechshagina, N. A., Konstantinov, Y. M., Kamenski, P. A. and Mazunin, I. O. (2018). Import of proteins and nucleic acids into mitochondria. *Biochemistry (Mosc.)* **83**, 643-661. doi:10.1134/S0006297918060032

Verechshagina, N., Nikitchina, N., Yamada, Y., Harashima capital En, C., Tanaka, M., Orishchenko, K. and Mazunin, I. (2019). Future of human mitochondrial DNA editing technologies. *Mitochondrial DNA A DNA Mapp. Seq. Anal.* **30**, 214-221.

Vergnolle, M. A., Sawney, H., Junne, T., Dolfini, L. and Tokatlidis, K. (2005). A cryptic matrix targeting signal of the yeast ADP/ATP carrier normally inserted by the TIM22 complex is recognized by the TIM23 machinery. *Biochem. J.* **385**, 173-180. doi:10.1042/BJ20040650

Wang, G., Chen, H.-W., Oktay, Y., Zhang, J., Allen, E. L., Smith, G. M., Fan, K. C., Hong, J. S., French, S. W., McCaffery, J. M. et al. (2010). PNPASE regulates RNA import into mitochondria. *Cell* **142**, 456-467. doi:10.1016/j.cell.2010.06.035

Wang, G., Shimada, E., Koehler, C. M. and Teitell, M. A. (2012). PNPASE and RNA trafficking into mitochondria. *Biochim. Biophys. Acta* **1819**, 998-1007. doi:10.1016/j.bbagrm.2011.10.001

Wang, G., Shimada, E., Nili, M., Koehler, C. M. and Teitell, M. A. (2015). Mitochondria-targeted RNA import. *Methods Mol. Biol.* **1264**, 107-116. doi:10.1007/978-1-4939-2257-4_11

Westermann, B. and Neupert, W. (2000). Mitochondria-targeted green fluorescent proteins: convenient tools for the study of organelle biogenesis in Saccharomyces cerevisiae. *Yeast* **16**, 1421-1427. doi:10.1002/1097-0061(200011)16:15<1421::AID-YEA624>3.0.CO;2-U

Wilcox, A. J., Choy, J., Bustamante, C. and Matouschek, A. (2005). Effect of protein structure on mitochondrial import. *Proc. Natl. Acad. Sci. USA* **102**, 15435-15440. doi:10.1073/pnas.0507324102

Wright, A. V., Sternberg, S. H., Taylor, D. W., Staahl, B. T., Bardales, J. A., Kornfeld, J. E. and Doudna, J. A. (2015). Rational design of a split-Cas9 enzyme complex. *Proc. Natl. Acad. Sci. USA* **112**, 2984-2989. doi:10.1073/pnas.1501698112

Yamano, T., Nishimasu, H., Zetsche, B., Hirano, H., Slaymaker, I. M., Li, Y., Fedorova, I., Nakane, T., Makarova, K. S., Koonin, E. V. et al. (2016). Crystal structure of Cpf1 in complex with guide RNA and target DNA. *Cell* **165**, 949-962. doi:10.1016/j.cell.2016.04.003

Zetsche, B., Gootenberg, J. S., Abudayyeh, O. O., Slaymaker, I. M., Makarova, K. S., Essletzbichler, P., Volz, S. E., Joung, J., van der Oost, J., Regev, A. et al. (2015). Cpf1 is a single RNA-guided endonuclease of a class 2 CRISPR-Cas system. *Cell* **163**, 759-771. doi:10.1016/j.cell.2015.09.038